Thermal performance and microclimate test methods for flat-plate solar thermal collectors

Anne Nykänen

M.Sc. Thesis in Applied Physics

University of Jyväskylä

Master's Degree Programme in Renewable Energy

Department of Physics

05.08.2012

Supervisor: Dr. Jussi Maunuksela

Preface

This Master's thesis marks the end to almost six years of university studies conducted in two different universities and countries. During this time I had the pleasure and honour to be accompanied by a great deal of wonderful people, some of which I will now mention here.

First of all a big Thank You to my supervisor Dr. Jussi Maunuksela, who guided me through this project with a great deal of patience and good advice. It was a pleasure working with you and learning from you!

I would also like to thank the people at Savosolar for their help with my research and for their smooth and friendly cooperation.

Another big Thank You is also owed to all my friends from the wind band Puhkupillit, and to Elina, Sabine, Stephanie, Susanne and Esa-Pekka, who have made life in Jyväskylä so cheerful and happy!

The starting point for all this however lies in Bonn, where I spent three years full of blood, sweat and tears to finally reach my Bachelor's degree in physics. Thank you to my friends from Bonn, especially Paul, Katja, Christoph and Stefan, for fighting together! Nina, your friendship and kindness shall never be forgotten.

Vielen Dank auch meiner ganzen Familie, meinen Eltern und meinen Brüdern, und ganz besonders auch meinen Freundinnen Karin und Amelie - ohne eure Unterstützung wäre ich wohl gar nicht über das erste Semester hinausgekommen!

Last but not least: Valtavat kiitokset Laurille rakkaudesta ja kärsivällisyydestä, olet paras!

Abstract

In this Master's thesis testing methods, experimental setups and data evaluation procedures for flat-plate solar thermal collectors are presented. An official quasi-dynamic test method according to the EU standard EN 12975 for evaluating the collector's thermal performance is described, and its applicability to an existing experimental setup is evaluated. The general practicality of this setup is also reviewed. Furthermore, a second experimental setup is designed to monitor the inside conditions, or microclimate, of a solar thermal collector, in order to assess the frequency of condensation occurrence inside the collector. This work's results include that the existing thermal performance setup needs to be upgraded in order to be able to produce accurate results, and that condensation inside the collector has not been observed during the whole measurement period. It can be concluded that the ventilation works well for the collector model in question.

Contents

Declaration of symbols

a_1, a_2	efficiency equation coefficients from collector specifications	W/(m^2· K)
A	(=A_a) collector aperture area	m^2
A_a	(=A) collector aperture area	m^2
A_A	collector absorber area	m^2
A_G	gross collector area	m^2
$b_1 ... b_n$	multiple linear regression coefficients	depends
c_1	collector heat loss coefficient at $T_m - T_a = 0$	W/(m^2· K)
c_2	temperature dependence of collector heat losses	W/(m^2· K^2)
c_3	wind speed dependence of collector heat losses	J/(m^3· K)
c_4	longwave irradiance dependence of the heat losses	-
c_5	effective thermal capacitance	J/(m^2· K)
c_6	wind dependence of the zero loss efficiency	s/m
C_{tyfo}	specific heat capacity of Tyfocor-water mixture	kJ/(kg · K)
C_w	specific heat capacity of water	kJ/(kg · K)
d	insulation thickness	m
E_L	incident longwave radiation	W/m^2
F'	collector efficiency factor	-
$F'(\tau\alpha)_{en}$	(= η_0) collector's zero-loss efficiency	-
G	solar irradiation (general variable)	W/m^2
G_b	beam solar irradiation on absorber	W/m^2
G_d	diffuse solar irradiation on absorber	W/m^2
G_{pyr}	total incident solar irradiation measured by pyranometer	W/m^2
G_{tot}	total incident solar irradiation on absorber	W/m^2
h_{b-a}	convective heat loss coefficient between collector back and ambient	W/(m^2· K)
h_{c-a}	convective heat loss coefficient between collector cover and ambient	W/(m^2· K)
h_{p-c}	convective heat loss coefficient between absorber plate and cover	W/(m^2· K)

$h_{r,b-a}$	radiative heat loss coefficient between collector back and ambient	W/(m^2· K)
$h_{r,c-a}$	radiative heat loss coefficient between collector cover and ambient	W/(m^2· K)
$h_{r,p-c}$	radiative heat loss coefficient between absorber plate and cover	W/(m^2· K)
k	heat conductivity of insulation	W/(m· K)
$K_{\theta b}$	incidence angle modifier for beam radiation	-
$K_{\theta d}$	incidence angle modifier for diffuse radiation	-
$\dot{m}$	heat transfer fluid mass flow rate	kg/s
m_w	mass of water	kg
n	node indicator / control variable in multiple linear regression	-
p_{fluid}	pressure at fluid inlet	Pa
$\dot{q}$	heat transfer fluid volumetric flow rate	m^3/s or l/h
$\dot{q_{act}}$	actual heat transfer fluid volumetric flow rate	m^3/s or l/h
$\dot{Q}_{exp}$	expected heating power	W
$\dot{Q}_{inst}$	instantaneous heating power	W
$\dot{Q}_u$	useful heating power	W
$\dot{Q}_{u,new}$	useful heating power according to modified equations (see section 3.1.4)	W
$\dot{Q}_{u,no\ wind}$	useful heating power according to modified equations without wind influence (see section 3.1.4)	W
t	time	s
T_a, T_{amb}	ambient temperature	°C (or K)
T_b	collector back temperature	°C (or K)
T_c	collector cover temperature	°C (or K)
T_{dew}	dew-point temperature	°C (or K)
T_{in}	collector inlet temperature	°C (or K)
T_m	mean absorber temperature	°C (or K)
$T_{n,f}$	final node temperature	°C (or K)
$T_{n,i}$	intial node temperature	°C (or K)

T_{out}	collector outlet temperature	°C (or K)
T_p	absorber plate temperature	°C (or K)
u	wind speed	m/s
U_b	collector bottom heat loss coefficient	W/(m^2· K)
U_e	collector edge heat loss coefficient	W/(m^2· K)
U_t	collector top heat loss coefficient	W/(m^2· K)
U_L	total collector heat loss coefficient	W/(m^2· K)
$x_1 ... x_n$	multiple linear regression dependent parameters	depends
y	multiple linear regression independent parameter	depends
z	percentage of full pump intensity	%
β	collector slope angle	°
γ	collector azimuth	°
ΔU_n	internal energy stored in storage tank node n	J
η	collector's instantaneous efficiency	-
η_0	$(=F'(\tau\alpha)_{en})$ collector's zero-loss efficiency	-
η_{spec}	collector's efficiency based on specifications	-
$\eta_{\text{spec},0}$	collector's zero-loss efficiency based on specifications	-
θ	angle of incidence of solar irradiation	°
ρ_{tyfo}	density of Tyfocor-water mixture	m^3/kg
ρ_w	density of water	m^3/kg
$(\tau\alpha)_{en}$	effective transmittance-absorptance product for direct radiation at normal incidence	-
$\omega_{rel,amb}$	ambient relative humidity	%
$\omega_{rel,in}$	relative humidity inside collector	%

1 Introduction

It has been predicted that the earth's major oil reserves are going to be practically exhausted by the year 2100 [1]. As a result, there is a growing need for and interest in renewable energy worldwide. Solar thermal collectors are an example of a renewable energy technology that harnesses solar energy [2]. This technology is spreading more and more, also throughout Nordic countries. In Finland, Savosolar, a company situated in Mikkeli, is manufacturing flat-plate solar thermal collectors with an innovative absorber coating permitting very high absorption efficiencies. More information on the coating is available on Savosolar's website [3]. The company's interest in their collectors' thermal performance and microclimate (*i.e.* inside air condition) behaviour during operation was the starting point for this thesis.

The main product of the Savosolar company is a single-glazed flat-plate solar thermal collector (see Fig. 1 for a typical solar collector cross section [4] and Fig. 2 for a photo of Savosolar's product). Its main part is a copper or aluminum absorber plate that includes fluid tubing. A fluid is circulated through the tubing in order to transport the collected heat away from the collector. The collector is connected to a closed fluid cycle from where heat is extracted with a heat exchanger to a storage tank. The storage tank is usually part of a secondary fluid cycle that enables using the collected heat *e.g.* for hot water production or air heating. A special absorber coating enables a very high absorption efficiency [3]. The absorber plate itself is placed inside a casing. The front side of the casing is closed with a glass plate that allows the solar radiation to reach the absorber and at the same time protects the plate from environmental influences like rain and dust. The space between glazing and absorber is ventilated with air coming through small holes in the side frame. An insulation layer is placed between the back of the absorber and the casing to reduce thermal losses.

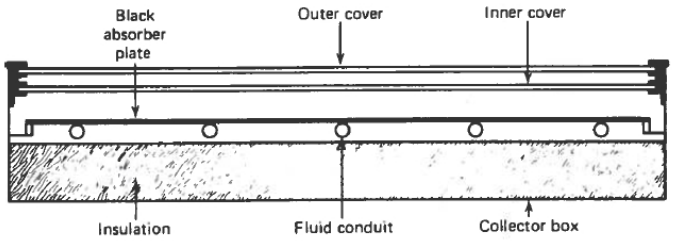

Figure 1: Cross section of a solar thermal collector with double glazing [4, Chap. 6]; NB: the collector referred to in this thesis has only one cover

In this thesis two main topics are studied: Thermal performance testing and microclimate testing of flat-plate solar thermal collectors. Thermal performance testing has evolved over the years, as the use of solar thermal collectors has grown more common. Starting out as research work done in universities or other research institutions, thermal performance testing is nowadays conducted using regionally standardized test methods. Standardized testing is necessary to ensure quality control and comparability of new products. A successfully passed thermal performance test is one of the requirements for receiving the European quality licence "Solar Keymark" [5]. This licence is well respected on the European collector market, which shows the importance of thermal performance testing for successful sales and marketing of solar thermal collectors.

One of the earliest standard testing methods available is the ASHRAE 93-77 standard used in North America [6]. Another important standard is the ISO 9806-1 [7]. Both of these standards use a so called steady-state method for thermal performance testing, which means that the collectors are tested in a carefully controlled environment. Irradiation, fluid inlet temperature and many other parameters are supposed to be kept stable within certain margins during the whole testing cycle. Such conditions are very hard to achieve using an outdoor test bench. For that purpose another testing method, quasi-dynamic testing, has been developed and is used in the European Standard SFS-EN 12975-2 [8, 9]. Quasi-dynamic testing is suitable for in- and outdoor testing alike and allows for more flexibility in the aforementioned parameter values. The standard testing for obtaining the Solar Keymark licence has to be performed according to the EN 12975 standard.

Microclimate testing is a rather small field compared to thermal performance testing and mainly conducted for collector research purposes. The purpose of microclimate testing is to monitor the temperature, relative humidity and pressure of the air inside the collector, and to assess the possible occurrence of condensation inside the collector. The ventilation and the insulation material have been identified as the main influencing factors on the condensation inside a solar thermal collector [10]. Computer simulations of the airflow through a collector similar to the Savosolar product were made by the author, investigating the most favourable ventilation option [11]. A comprehensive work on different collector microclimate studies is available by M. Köhl *et al.* [12]. As background information for these two main topics the basic principles of solar thermal collectors [4] and heat transfer processes [13] are presented.

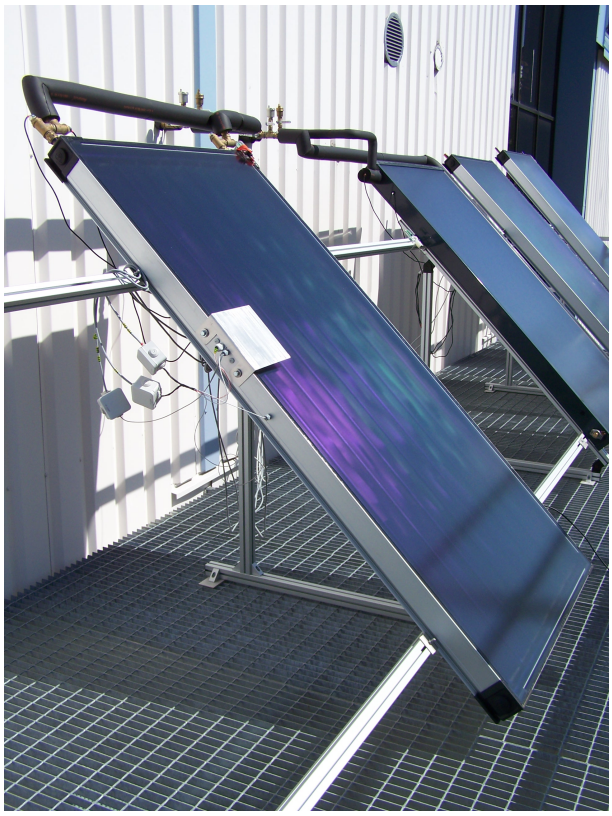

Figure 2: A photograph of Savosolar's solar thermal collector test bench; a part of the collector test installation can be seen on the left side of the collector

This work is intended to give an overview over methods to test and evaluate a solar thermal collector's thermal performance and microclimate. In addition, it describes two measurement setups that were used for collector testing, and results from the measurements. Savosolar's existing experimental setup and its suitability for thermal performance testing was assessed based on the performance test procedure explained in this work. The method follows to some extent the European Standard EN 12975-2 for test methods of thermal solar systems. The experimental setup is not intended for standardized testing, but it can be used to assess the collector's thermal performance. A second experimental setup was used to determine condensation taking place on the inside of Savosolar's collector. For this purpose several sensors were placed inside a collector to monitor the inside air temperature and humidity conditions over a time span of several months.

2 Theoretical background

The aim of this chapter is to familiarize the reader with the physical processes involved in this study, and to give an introduction to thermal performance test methods for solar thermal collectors.

2.1 Heat transfer processes

Energy harvest with solar thermal collectors is based, like the name already suggests, on collecting heat from incoming solar radiation. In order to utilize the collected heat in an efficient way, heat transfer processes happening in and around the collector need to be analyzed and understood.

In general heat transfer consists of three main modes (Fig. 3): conduction, convection and radiation. The propagation of heat via molecular movements in gases or liquids is called conduction. In solid bodies heat conduction functions through lattice vibrations. Convection is defined as the heat transport in a fluid (gas or liquid) which happens at the fluid's own flow velocity. Another form of convection is heat dissipation from a solid surface to a fluid. Finally, radiation refers to heat transfer that happens via photon exchange. Where ever a temperature difference is present, heat transfer occurs until a thermal equilibrium is established [13, Chap. 1].

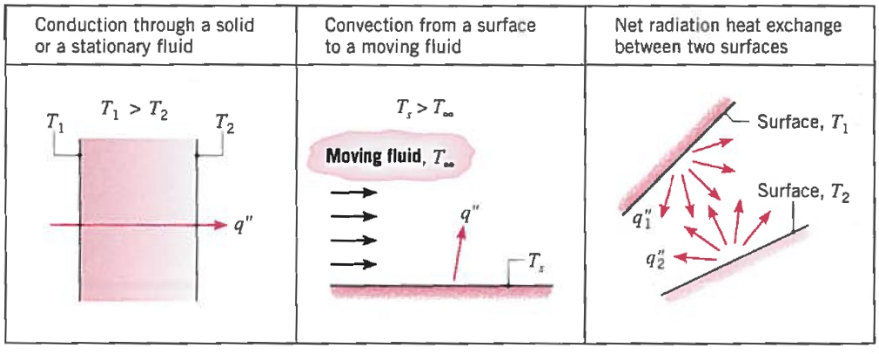

Figure 3: Three drawings illustrating the concepts of conductive, convective and radiative heat transfer [13, Chap. 1]

There are several heat transfer meachanisms at work in a single-glazed flat-plate solar thermal collector. Heat is gained via solar irradiance. The total solar irradiation that reaches

the absorber after passing the glass cover (where reflection and absorption losses occur) is denoted by G_{tot}. Heat losses occur in a controlled way via the extraction of useful heat ($\dot{Q}_u$) by conduction, and in uncontrolled ways via top (U_t), bottom (U_b) and edge losses (U_e) by convection and radiation. Top losses refer to the losses through the glazing, bottom losses to the losses through the back of the collector casing. A cross section and a thermal network drawing for the collector model in question is shown in Fig. 4.

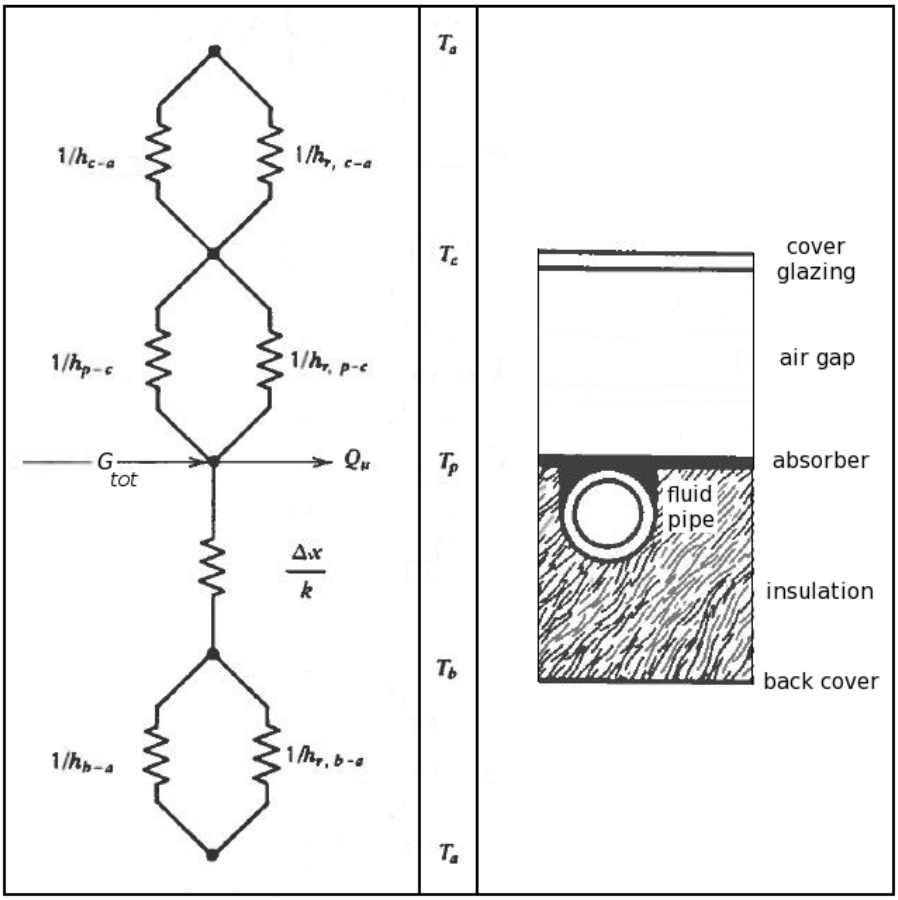

Figure 4: Depicted on the left is a thermal network, on the right the corresponding cross section of a solar thermal collector; the temperature indicator in the middle assigns the right temperature variable to each part of network and collector (adapted from [4, Chap. 6]).

The incoming solar irradiance G_{tot} (which is the indicent solar radiation on the collector minus the occuring reflection and absorption losses on the glass cover) warms up the absorber, and via the heat exchange fluid circulating the pipes the useful heat $\dot{Q}_u$ is removed. The top losses consist of radiational heat transfer between the absorber plate and the cover described by the heat transfer coefficient $h_{r,p-c}$, and between the cover and the ambient described by

$h_{r,c-a}$. The air gap between absorber and cover plate as well as the ambient air facilitate convective heat transfer, *i.e.* losses represented by the heat transfer coefficients h_{p-c} and h_{c-a}. Through the insulation on the back heat is lost via conduction from the absorber plate to the surrounding air (d/k, where d is the thickness of the insulation and k its conductivity); on the boundary between back casing and ambient air radiative and convective losses are also present ($h_{r,b-a}$ and h_{b-a}). Losses through the sides (edges) of the collector are always occurring, but in our case negligbly small as the metallic frame construction is sufficiently air-tight and insulated [$U_e \approx 0$ W/(m$^2 \cdot$ K)]. Important temperatures in this model are the ambient (T_a), cover (T_c), plate (T_p) and back casing temperature (T_b). Cover, plate and back casing temperatures depend on ambient temperature, solar irradiance and the collector's heat transfer coefficients. A new variable, the collector overall loss coefficient U_L, can be introduced to include all aforementioned losses:

$$\begin{aligned} U_L &= U_t + U_b + U_e \\ &= \Big(\frac{1}{h_{p-c} + h_{r,p-c}} + \frac{1}{h_{c-a} + h_{r,c-a}}\Big)^{-1} + \Big(\frac{1}{h_{b-a} + h_{r,b-a}} + \frac{d}{k}\Big)^{-1} + 0, \end{aligned} \tag{1}$$

where "0" refers to the edge losses that were assumed to be negligible.

In order to utilize a flat-plate collector it has to be part of a system that includes piping, at least one fluid storage tank and an optional heat exchanger located inside the storage tank (*cf.* Fig. 5). The heat exchanger enables heat flow between the primary and the secondary fluid cycle. The system in our case works as follows: The fluid circulating the collector transfers the heat to a heat exchanger inside a storage tank. A secondary cycle transports the heat from the storage tank to the point where it is used (here in an air heating device). The heat exchange fluid used in the cycles can be *e.g.* water, but a more common choice is a mixture between water and Tyfocor, a liquid based on ethylene glycol. Its advantage is a lower freezing point in comparison with water, which simplifies running the collectors during the winter. Heat losses are occuring in all parts of the system, and it is recommended that as many components as possible should be insulated. Especially pipe losses can thus be drastically reduced.

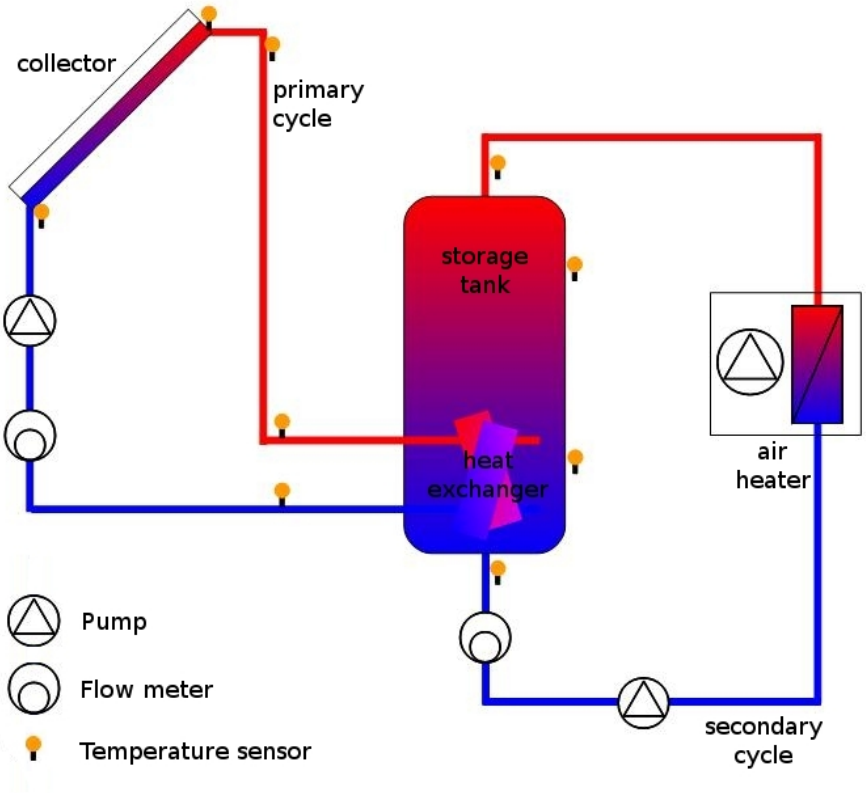

Figure 5: A schematic of a solar heat collection system (adapted from Savosolar's presentation slides); the positions of temperature sensors, pumps and flow meters for performance testing are indicated.

2.2 Microclimate

The microclimate of a solar thermal collector is defined by the temperature, pressure and relative humidity in the air gap between the cover and the absorber (*cf.* [12, Chap. 3.1]). These parameters indicate when conditions allow for condensation to form on the inside of the collector glazing, or worse, on the absorber plate. A condition for the formation of condensate inside the collector is that the temperature of the cover glazing is below the dew-point temperature of the inside air. Another indicator for the possiblity of condensate to form is if the inside air relative humidity is higher than the outside air relative humidity. Condensation inside the collector should be avoided as it leads to corrosion and lowered collector efficiency (immediate and long-term). Therefore it is sensible to have a closer look at the microclimate, and at ways to change it, if necessary.

There are two ways to influence the microclimate - choosing an appropriate insulation material that does not absorb water vapour and thus does not collect condensate, and ventilating the collector sufficiently. In our case the insulation material chosen by the manufacturer has proven to be suitable - a small series of tests showed that the material allows water to evaporate very quickly and does not store it. Thus the main purpose of microclimate monitoring in this study is to eventually determine how to ventilate the collector so that condensation is minimized. For further details on the topic of microclimate refer to the research training report written by the author [11].

According to literature [10] and to a computational study made by the author [11] the most favourable way of ventilating a collector is diagonally, meaning that there should be two ventilation holes in diagonally opposite corners of the collector (Fig. 6). The manufacturer's collector has in total eight openings (two in every corner), and for this study six of them were sealed in order to enable said diagonal air flow. This setup was used as the starting point for the measurements. The other possible ventilation setup is to open holes in all four corners. The computer simulations showed however that this setup is not as good as the two-hole ventilation, as it accumulates more moisture inside the collector. This can be explained using a result by Köhl *et. al.* [10], which shows that the air inside the collector casing usually has a lower relative humidity than the surrounding air. Based on this finding it is logical to conclude that a higher air exchange between the collector casing and the surroundings caused by a bigger number of open ventilation holes results in more moisture entering the collector.

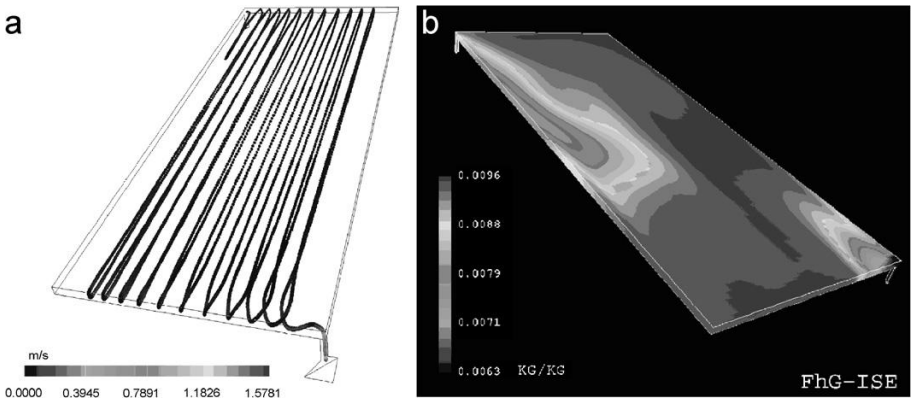

Figure 6: A computational fluid dynamics (CFD) simulation showing the diagonal air flow through a solar thermal collector [10]

2.3 Thermal performance test methods

Before a solar thermal collector is made available for purchase a number of tests has to be conducted. These include among others durability, safety, reliability and performance tests. Several test standards such as the ISO 9806, the ASHRAE 93 (North America) and the European EN 12975 standard provide generalized procedures to characterize solar thermal collectors [6, 7, 8]. Testing according to these standards needs to be conducted in certified test laboratories, from where official test certificates, *e.g.* the Solar Keymark licence, can be obtained. For more information on the Solar Keymark licence see their website [5].

The thermal performance of a solar thermal collector, including among other things conversion efficiency and effective thermal capacitance, is traditionally tested under steady-state conditions. This requires several parameters like collector inlet and outlet temperature T_{in} and T_{out}, ambient air temperature T_a, wind speed u, incident global solar irradiance G_{tot} (on absorber, after reflection losses of cover) and its angle of incidence θ to be constant within certain margins. For outdoor steady-state testing clear-sky conditions with little diffuse irradiance are required (under 30% of total irradiance [8, Chap. 6.1.4.3]). The EN standard however also includes a quasi-dynamic test procedure which is intended for outdoor testing under less strict circumstances than the steady-state method.

The EN Standard 12975-2 "Thermal solar systems and components. Solar collectors. Part 2: Test methods" includes a description on how to perform quasi-dynamic collector testing [8, Chap. 6.3]. The procedure is structured so that data meeting the more strict requirements of the steady-state measurements can be extracted. A short summary of the quasi-dynamic test procedures with a focus on outdoor testing is given below:

Positioning the collector

The first thing to be taken care of before measuring is the correct placement of the collector. According to chapters 6.1.1 and 6.3.1. of the EN standard the collector has to be mounted so that the mount does not obstruct the collector's aperture and that there are no shadows cast on the collector. Furthermore, a maximum of 5% of the collectors field of view can be obstructed. Reflections from surrounding buildings have to be avoided, as well as thermal radiation sources (*e.g.* hot air exhausts) in the close vicinity. The collector needs to be at least 0,5 m above the ground level. The slope angle β is supposed to be less than 20°, but for

most collectors the influence of the slope angle is rather small. The collector should face the equator with an allowed azimuthal deviation of ±5°. Air is supposed to pass freely around the collector structure.

Measuring equipment

In general the measuring equipment is required to have an accuracy of 1% of the measured value (digital devices), or the smallest division of the instrument should be no more than two times as high as the specified accuracy for the measurement in question (analog devices). More details on the necessary device specifications can be found in chapter 6.1.2.7 of the standard.

In order to measure the solar irradiance a class I pyranometer has to be mounted in the same plane as the collector (with the same slope). The angle of incidence of the solar irradiance should be measured (see chapter 6.1.2.1.2 of the standard for instructions). If the collector's performace is suspected to be sensitive to thermal irradiance this parameter can be monitored using a pyrgeometer.

The fluid temperature is to be measured at the collector inlet and outlet. The accuracy of these measurements is supposed to be ± 0,1 K or better. The sensors have to be mounted less than 20 cm away from the inlet/outlet point. The ambient air temperature is to be monitored with an accuracy of 0,5 K. The sensor should be positioned inside a shelter and in a shaded place, no more than 10 m away from the collector and at least 1 m above the ground. Air speed shall be measured with an accuracy of at least 0,5 m/s in the case of glazed collectors. The pressure at the fluid inlet of the collector (and possibly the pressure drop across the collector) should be measured. The accuracy for this measurement is supposed to be ±10 Pa or 5 % of the measured value (for digital devices).

The amount of fluid that can be kept inside the collector should be known within 10 % uncertainty. The uncertainty of fluid mass flow rate needs to be within 1 % of the measured value, and it needs to be kept stable throughout a test sequence. The specific heat capacity and density of the fluid are required to be known over the whole temperature range with an accuracy of ± 1 %. Finally, the collector area is to be known with an error of less than 0,3 %.

Collector test loop

An example of a closed test loop is shown in Fig. 7. Details about the necessary specifications for pipework, pumps and flow measurement devices can be found in chapter 6.1.3 of the standard. A very important requirement for each test sequence is that the collector fluid inlet temperature is kept constant at the desired value during the whole sequence.

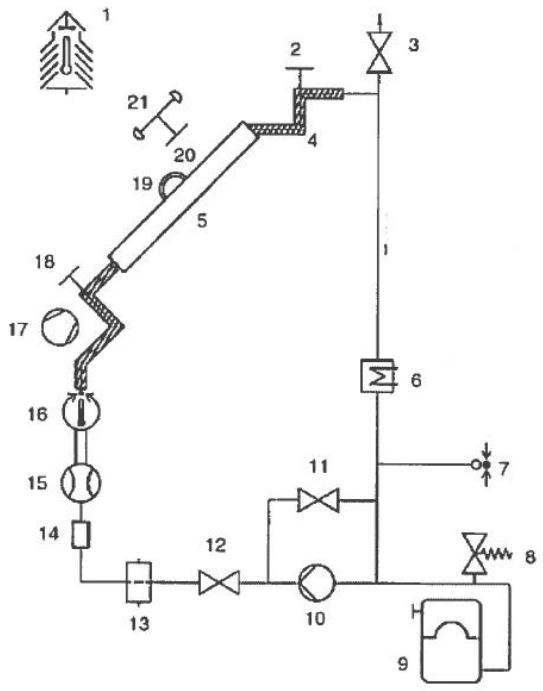

Key

1 Surrounding air temperature sensor
2 Temperature sensor (t_e)
3 Air vent
4 Insulated pipe
5 Solar collector
6 Heater/cooler for primary temperature control
7 Pressure gauge
8 Safety valve
9 Expansion tank
10 Pump
11 Bypass valve
12 Flow control valve
13 Filter (200 µm)
14 Sight glass
15 Flowmeter
16 Secondary temperature regulator
17 Artificial wind generator
18 Temperature sensor (t_{in})
19 Pyrgeometer
20 Pyranometer
21 Anemometer

Figure 7: A closed test loop [8, Chap. 6.1.3.1]

Table 2: Necessary measurement parameters in a thermal performance setup for EN standard testing

parameter	variable
collector aperture area	A_a
absorber area	A_A
gross collector area	A_G
collector's liquid content	-
global solar irradiance	G_{tot}
diffuse solar irradiance	G_d
incident longwave radiation	E_L
(angle of incidence of solar radiation	θ)
collector azimuth	γ
collector slope angle	β
air speed	u
ambient temperature	T_a
heat transfer fluid temperature at inlet	T_{in}
heat transfer fluid temperature at outlet	T_{out}
flowrate of heat transfer fluid	$\dot{m}$
pressure at fluid inlet	p_{fluid}

Measurement conditions and procedure

Several test conditions need to be met in order to produce valid test data. The total irradiance on the collector should be greater than 700 W/m^2. The wind speed needs to be between 1 m/s and 3 m/s, and the fluid flow rate should be set to 0,02 kg/s per square meter of collector area. Test sequences for at least four different inlet temperatures should be measured, one being close to ambient temperature in order to measure the zero loss efficiency η_0 (collector efficiency at mean temperature $T_m = T_a$, where $T_m = (T_{in} + T_{out})/2$). The parameters listed in Tab. 2 are to be measured when conducting a collector test according to the EN standard.

The collector aperture area A_a describes the size of the aperture through which radiation enters the collector, *i.e.*, the size of the glazing disregarding the parts covered by the frame

construction. The absorber area A_A is the whole area of the absorber, and the gross collector area A_G refers to the measures of the whole collector construction.

The data sampling rate should be between 1 s and 6 s, and the averaging interval between 5 min and 10 min. A time label should be recorded for each parameter/data line. Furthermore, with the same sampling rates and averaging intervals, two on line calculations should be conducted to find the useful output power $\dot{Q}_u$ and the time derivate of the mean fluid temperature dT_m/dt. The recommended amount of outdoor test days should be about 4-5. This refers to days in which the test conditions are satisfactory, the actual number of days during which data needs to be collected may be significantly higher. Each test sequence should at the minimum be 3 hours long. Data from one partially cloudy day is to be included in the test evaluation in order to get a set of data where the values of the time derivate of the mean fluid temperature dT_m/dt are high enough to estimate its influence.

More information on the correct data evaluation and presentation (*e.g.* in standardized forms) can be found in the standard (Chapters 6.3.4.6.4 and 6.3.4.7); they are not explained here as the handling of data in this thesis will differ from the standard requirements.

Modeling of the collector's thermal performance

Eq. 2 models the useful energy output per collector area (gross, aperture or absorber area) [8, Chap. 6.3.4.8]:

$$\begin{aligned}\frac{\dot{Q}_u}{A} =& F'(\tau\alpha)_{en}K_{\theta b}G_b + F'(\tau\alpha)_{en}K_{\theta d}G_d - c_6 u G_{tot} - c_1(T_m - T_a) - c_2(T_m - T_a)^2 \\ & - c_3 u(T_m - T_a) + c_4(E_L - \sigma T_a^4) - c_5\frac{dT_m}{dt}. \end{aligned} \tag{2}$$

The first two terms on the right hand side of the equation describe the incident direct beam (subscript b) and diffuse (subscript d) radiation on the absorber. In these terms G stands for the incident solar irradiance and K_θ for the incidence angle modifier that is described more closely in section 2.3. The zero loss efficiency $F'(\tau\alpha)_{en}(= \eta_0)$ consists of the collector efficiency factor F' and the effective transmittance-absorptance product for direct radiation at normal incidence $(\tau\alpha)_{en}$. Because the zero loss efficiency $F'(\tau\alpha)_{en}$ or η_0 is a parameter well accessible by measurements, a further explanation of its parts shall be left out. More information on them can be found in Duffie's book [4, Chap. 6].

The next terms describe various losses and gains that are not covered by the first two

terms. The influence of the wind speed u is accounted for in two terms. In those, c_6 stands for the wind dependence of the zero loss efficiency, and c_3 for the wind speed dependence of the heat losses. Temperature dependent heat losses are also included in two terms, c_1 being the heat loss coefficient at $T_m - T_a = 0$ and c_2 being the temperature dependence of the heat losses. Losses due to temperature changes over time are represented by the last term, consisting of the mean temperature time derivative dT_m/dt and the effective thermal capacitance c_5. Finally, an additional gain is provided by the long-wave irradiance, where c_4 is the long-wave irradiance dependence of the heat losses, E_L the incident long-wave radiation and σ the Stefan-Boltzmann constant.

The terms with coefficients c_3, c_4 and c_6 (and only those) may be left out due to insignificance. In order to check whether that is the case, their values and standard deviations are interpolated from the available data. Then their T-ratio, being the ratio of parameter value and standard deviation, shall be calculated. If this ratio is smaller than 2, the term can be discarded. Then the other parameters need to be determined again. In order to identify the thermal capacitance c_5 data for a large enough span of different irradiances needs to be recorded, so that the value for dT_m/dt exceeds 0,005 K/s. Such conditions are usually met during a cloudy test day.

Incidence angle modifier

The incidence angle modifier for direct radiation $K_{\theta b}$ and the one for diffuse radiation $K_{\theta d}$ are collector parameters that need to be identified from data. They show the dependence of the collector's performance on the radiation's angle of incidence. This is relevant information for modeling the collector's energy output throughout the day. $K_{\theta d}$ is treated as a collector constant and directly interpolated from data, whereas for $K_{\theta b}$ the following relation is to be evaluated:

$$K_{\theta b} = 1 - b_0\Big(\frac{1}{\cos\theta} - 1\Big) \tag{3}$$

In this equation θ stands for the angle of incidence, and b_0 is a collector constant helping with modelling the incidence angle modifier. For determining the incidence angle modifiers a whole test day shall be reserved [8, Chap. 6.3.6].

Time constant measurements

Measuring the collector's time constant is an optional, but a quite useful procedure [8, Chap. 6.1.6.3]. The time constant shows how quickly the collector reacts to irradiance changes.

The solar irradiance during the test time has to be greater than 700 W/m^2. The fluid flowrate should be the same as in other tests, and the fluid inlet temperature should be close to ambient temperature. A cover is now installed to shield the collector from the sunlight. Once a steady state has been reached, the cover is removed and then the measurement is continued until steady state conditions are again reached. Steady state means here that the temperature change in the outlet temperature is less than 0,05 K per minute. The measured parameters are inlet, outlet and ambient temperature (T_{in}, T_{out} and T_a). The time constant is defined as the time between removal and the point where the difference between outlet and ambient temperature has risen to 63,2 % of its final value.

Summary of conditions

A summary of all conditions for quasi-dynamic collector testing according to EN 12975 can be found in Tab. 3.2.1 in chapter 3.2.1. A good overview over the topic and the required conditions for quasi-dynamic collector testing is given in [9].

3 Experimental setups

In this chapter Savosolar's experimental setup for thermal performance testing is described, and a testing method is proposed. A comparison of the quasi-dynamic test requirements with the present setup serves as a means of evaluating how well the results can be trusted, and where caution in their interpretation needs to be exerted. The closer the test conditions are to the requirements of the standard, the more comparable are the results to other collectors' specifications. An improvement of the standard method's heat output modeling is proposed, which is fitted to the circumstances of the setup at hand. Furthermore, the microclimate measurement and data acquistion system is described.

3.1 Test bench

Savosolar's test bench is designed to study two flat-plate collectors simultaneously. Each of these collectors is connected to their own primary heat transfer fluid cycle. A setup schematic for each collector is shown in Fig. 9. There is however only one secondary fluid cycle which includes both storage tanks and fluid heat exchangers. Subsequently there is also only one air heater which uses the collected heat to warm up the air in Savosolar's production hall. The test bench is situated on a support on the factory's south-facing wall. Its deviation from exact south is $\Delta\gamma < 5$ °. The collectors' slope angle equals to $\beta \approx 45$ °. A photograph of the test bench is shown in Fig. 2.

3.2 Thermal performance testing

Savosolar's setup for thermal performance testing uses the solar process control system Delta-Sol MX, accompanied by datalogger DL2, by the company RESOL for collecting data. It is meant for constant monitoring of the collector system's parameters, rather than for accurate performance testing purposes. Two solar thermal collectors are connected to the test bench system, Savosolar's own model (SF-100-02, aluminum absorber with copper tubing [14]) and one of the company KBB (K420MS-AL, also aluminum absorber with copper tubing [15]). The collectors' absorber, aperture and gross areas are listed in Tab. 3. For the error calculation a length measurement error of 1 mm was assumed for the Savosolar collector. The error for the KBB collector is not known. The collectors' tubing pattern and the way the fluid

takes through the pipes is shown in Fig. 8. In the KBB collector the fluid is led through one meandering tube, which is wound across the whole absorber starting in the upper left corner and ending in the lower left corner. In the Savosolar collector a U-shaped pattern is used, where the fluid enters in the upper left corner, the finds its way down through several parallel tubes on the left side of the absorber to a bigger conduit at the bottom. This conduit leads the fluid to the right side of the absorber, up again through several parallel tubes and out through the upper right corner.

Table 3: Area and liquid content values for Savosolar and KBB collector

	Savosolar SF-100-02	KBB K420MS-AL
absorber area	1,98 m^2 ($\pm$ 2,8 %)	2,00 m^2
aperture area	2,00 m^2 ($\pm$ 2,7 %)	2,00 m^2
gross collector area	2,18 m^2 ($\pm$ 2,6 %)	2,15 m^2
liquid content	1,9 l	1,7 l

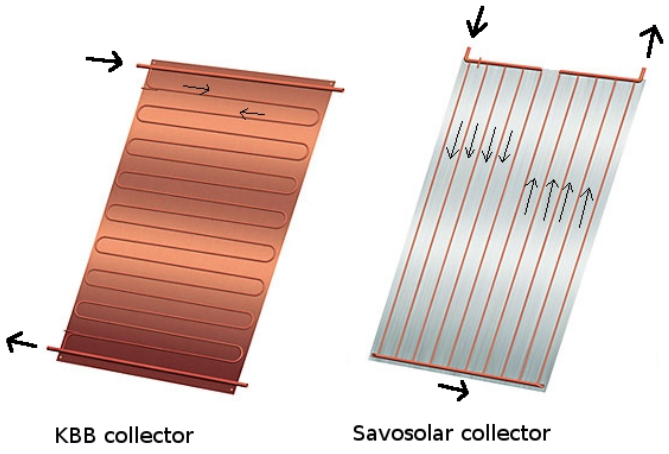

Figure 8: A schematic showing the absorber piping and fluid flow paths for KBB and Savosolar collectors. The pictures are based on drawings from KBB's homepage, so the Savosolar collector drawing is only a sketch showing the general idea of the flow pattern. The color of the KBB absorber indicating the use of copper might be misleading - in fact, both collectors have an aluminum absorber with copper tubing.

The temperature and flow sensors used in the setup (Fig. 9) and their descriptions are listed in Tab. 4. The pumps in the cycles are denoted with R1a (Savosolar primary cycle), R1b (KBB primary cycle) and R2 (secondary cycle). The fan that enables air flow through the air heater is called R3. The pumping power as a fraction of the full power (in %) is also used as a parameter and estimated via the RESOL datalogger. Because the fluid flow in the primary cycle is lower than the sensitivity of the flow meter, a constant flow rate of $\dot{q} = 70$ l/h was suggested to be used for the calculation.

Table 4: Sensors used in thermal performance test setup

measured parameter	sensor name	accuracy	number in Fig. 9
absorber temperature	RESOL FKP 6	± 0,8 °C	S1
collector inlet temperature T_{in}	RESOL FKP 6	± 0,8 °C	S7
collector outlet temperature T_{out}	RESOL FKP 6	± 0,8 °C	S6
storage tank lower part temperature	RESOL FKP 6	± 0,8 °C	S2
storage tank upper part temperature	RESOL FKP 6	± 0,8 °C	S3
storage tank inlet temperature	RESOL FKP 6	± 0,8 °C	S9
storage tank outlet temperature	RESOL FKP 6	± 0,8 °C	S8
heat exchanger inlet temperature	RESOL FKP 6	± 0,8 °C	S4
heat exchanger outlet temperature	RESOL FKP 6	± 0,8 °C	S5
ambient temperature	RESOL FKP 6	± 0,8 °C	S10
ambient temperature	RESOL FKP 6	± 0,8 °C	S11
ambient/collector's backside temperature	RESOL FKP 6	± 0,8 °C	S12
solar irradiance intensity	solar cell CS10	?	CS10
Savosolar primary cycle flow	V40-06	?	IMP1a
KBB primary cycle flow	V40-06	?	IMP1b
secondary cycle flow	V40-06	?	IMP2
Savosolar primary cycle pump power (in %)	Wilo Star RS15/6	N.A. (on/off)	R1a
KBB primary cycle pump power (in %)	Wilo Star RS15/6	N.A. (on/off)	R1b
secondary cycle pump power (in %)	Grundfos Alpha 2	N.A. (on/off)	R2

Table 4: Continued from previous page

measured parameter	sensor name	accuracy	number in Fig. 9
air heater pump power (in %)	VTS Euroheat Volcano	N.A. (on/off)	R3

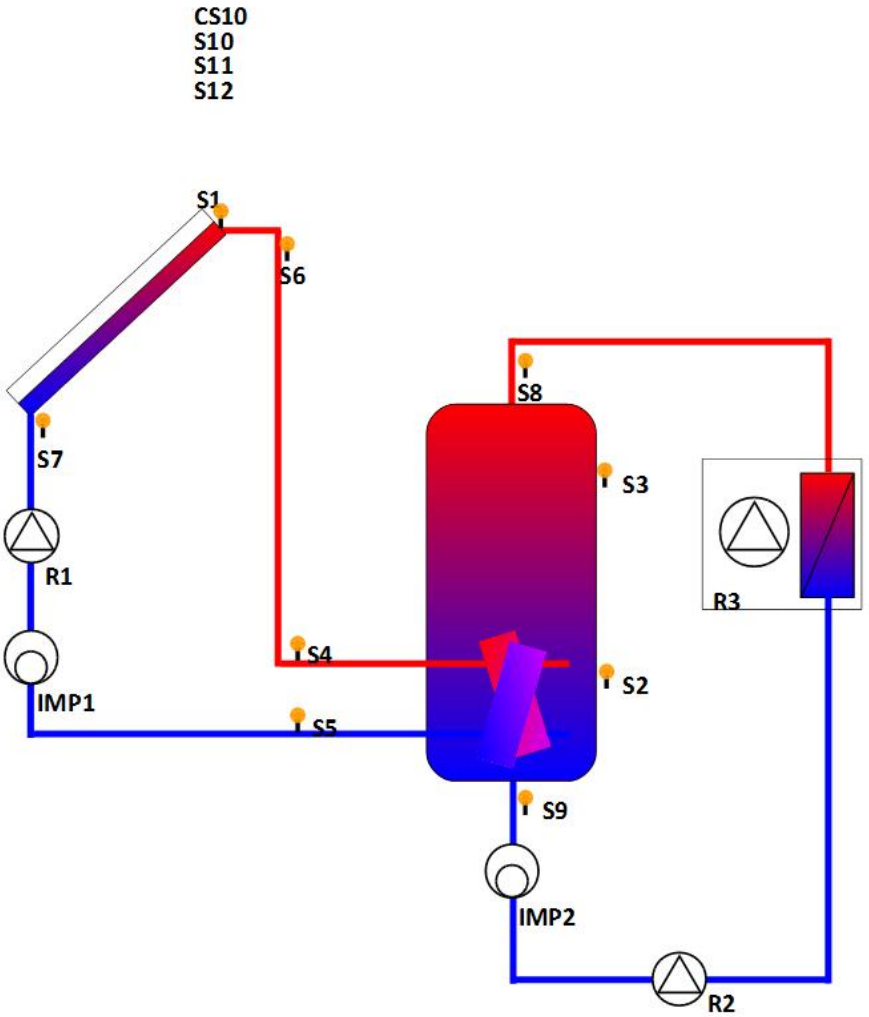

Figure 9: A schematic of Savosolar's heat collecting system; a list of sensors and corresponding numbers can be found in Tab. 4. The pump R1 stands for either R1a (Savosolar collector cycle) or R1b (KBB collector cycle), the same goes for the flowmeter IMP1 and the primary cycle temperature sensors. The picture was taken from Savosolar's presentation slides.

The heating cycle begins when the primary cycle pump R1 starts up, *i.e.*, the temperature difference between the collector and the lower part of the storage tank grows bigger than 6 °C. The pump shuts down, when the difference falls below 4 °C. A water-Tyfocor mixture is used as a heat transfer liquid in the collectors' primary cycle, the secondary cycle runs on water. The Tyfocor concentration in the primary cycle of the Savosolar collector was determined to be about 34%. This result was obtained from Tyfocor's specifications [16] using the measured density value of 1,027 g/cm^3 at a temperature of 31 °C. Similarly the concentration in the primary cycle of the KBB collector was estimated to be 44 % for a density of 1,034 g/cm^3 at 35,5 °C.

The secondary or heat rejection cycle pump R2 is controlled by a timer, letting it run from 19:00 until 04:30 in the morning. At the same time the air heater is used to dump the stored heat into the production hall for room heating, thus cooling down the liquid in the secondary cycle. The liquid used in the secondary cycle is water. The primary and secondary pumps don't run at the same time due to the way the system was designed. During the day the heat is collected in the tanks, then the primary pumps are switched off in the early evening due to the temperature difference between collector in- and outlet temperature falling below the critical value. The secondary cycle starts up at 19:00, releasing the heat into the building via the air heater during the night.

A pyranometer was included in the setup to measure solar irradiance (more information in section 3.3). The irradiance measured by the pyranometer is not equal to the incident radiation on the absorber G_{tot}, as the transmittance of the glass cover is for both collectors approximately 92 % (*cf.* [14] and [15]). The irradiance data is crucial for determining *e.g.* the collector's efficiency. Included in the setup is RESOL's CS10 sensor, which consists of a small solar cell inside a transparent round casing. In our case the casing was replaced with a small glass dome; the dome has a better shape for letting irradiance pass to the sensor also from the sides. The cell's irradiance-current-relation was already programmed to RESOL's data-logger. The spectral sensitivity or the general accuracy of the cell is not known. The sensor CS10 provides a rough estimate on the incoming radiation. A pyranometer is a much more accurate device that is sensitive also for diffuse radiation, and has an even spectral response over a large part of the solar spectrum. Thus it can also be used to determine to what extent the less accurate CS10 sensor can be trusted.

A wind speed measured was meant to be included into the setup as well, but couldn't be implemented due to a malfunction of the wind speed sensor (see also section 3.3).

Data acquisition

The data from the aforementioned sensors was recorded using the datalogger DL2 by RESOL. Data files can be downloaded from the device's memory. For each day one output file was created, including data from all sensors for each minute of the day, a time stamp and an error note. From these data files the adequate data for collector characterization has to be filtered. More information on the data selection can be found in chapter 4. The pyranometer's data is averaged and recorded for every minute of the day with the microclimate setup (*cf.* section 3.3), so the data for both setups can be compared easily.

3.2.1 Thermal performance setup compared to the EN standard

Since the test bench and the measurement setup were designed for monitoring the day-to-day operation of solar collectors they do not conform with all the requirements given by the EN standard for collector testing. Table 5 lists the requirements set by the standard and whether or nor the experimental setup fulfills these requirements.

Table 5: Quasi-dynamic test conditions and their fulfillment by the measurement setup

condition	met by setup?
POSITIONING	
no shadows cast on collector during whole day	no (railing)
less than 5% of viewfield obstructed	yes
avoid reflections from surroundings	no (white factory wall)
avoid thermal radiation sources	yes
collector at least 0,5 m above the ground	yes
slope angle β less than 20°	no (but only small influence)
collector faces south with azimuth (γ) deviation $\leq$5°	yes
air flows free around collector	yes

Table 5: Continued from previous page

condition	met by setup?
EQUIPMENT	
measurement equipment's general accuracy of 1%	no (*e.g.* FKP6 sensors)
class I pyranometer	no (secondary standard)
thermal irradiance measurement	no
collector aperture area A_a known with under ± 3% error	Savosolar: yes, KBB: no
absorber area A_A known with under ± 3% error	Savosolar: yes, KBB: no
gross collector area A_G known with under ± 3% error	Savosolar: yes, KBB: no
collector's liquid content known with an accuracy of ± 10%	yes
specific heat capacity and density of heat transfer fluid known over whole temperature range with an accuracy better than ± 1%	yes
MEASUREMENTS	
global solar irradiance $G_{tot} \geq 700$ W/m^2	yes (for selected data)
diffuse solar irradiance G_d less than 30 % of total irradiance	no (N.A.)
incident longwave radiation E_L measured	no
angle of incidence of solar radiation θ measured	no
air speed u between 1 m/s and 3 m/s and accuracy better than ± 0,5 m/s	no (N.A.)
ambient temperature T_a with accuracy better than ± 0,5 K, positioning correct	no (positioning ok)
heat transfer fluid temperature at inlet T_{in} with accuracy better than ± 0,1 K	no
heat transfer fluid temperature at outlet T_{out} with accuracy better than ± 0,1 K	no
flowrate of heat transfer fluid $\dot{m}$ known with uncertainty of less then 1%	no (N.A.)
pressure p_{fluid} known with an accuracy of ± 10 Pa	no

Table 5: Continued from previous page

condition	met by setup?
collector inlet temperature T_{in} kept stable	no
four different inlet temperatures tested	no
sampling rate between 1 s - 6 s	no (N.A.)
averaging to 5 min - 10 min intervals	yes, possible
data lines have time labels	yes
on-line calculations for $\dot{Q}_u$ and mean temperature time derivative dT_m/dt	no
amount of test days: 4-5, with at least 3h sequences	see chapter 5
for one cloudy test day $dT_m/dt \geq 0{,}005$ K/s	see chapter 5

As is evident, many conditions are not met by the setup. Thus, the results of this thesis can give a good idea about the collector's performance, but they cannot be compared directly to other companies' collector specifications. However, the test setup can be used for direct comparison of two different collectors, in this case the Savosolar collector and the KBB collector.

3.2.2 Modeling the heat output

The available measurements do not provide data for all the parameters in Eq. 2, so it has to be simplified. In this case the simplification was done in two steps, first a more simple equation including the influence of the wind speed was found, and in the second step also the wind dependence was left out of the equation. These simplified equations are presented as follows:

$$\begin{aligned}\frac{\dot{Q}_{u,new}}{A} =& F'(\tau\alpha)_{en}K_\theta G_{tot} - c_6 u G_{tot} - c_1(T_m - T_a) - c_2(T_m - T_a)^2 \\ & - c_3 u(T_m - T_a) - c_5\frac{dT_m}{dt} \qquad (4)\end{aligned}$$

$$\frac{\dot{Q}_{u,no\ wind}}{A} = F'(\tau\alpha)_{en}K_\theta G_{tot} - c_1(T_m - T_a) - c_2(T_m - T_a)^2 - c_5\frac{dT_m}{dt}. \qquad (5)$$

The changes that were introduced to get from Eq. 2 to the Eqs. 4 and 5 are described in more detail in this paragraph: Although calculational models for finding the diffuse part of the radiation exist (see [4, Chapter 2.10]), they cannot be applied in this case. The influence of the white factory wall on the diffuse radiation part is probably rather high, so the models, which are devised for a setup without immediate surroundings, are not valid here. Thus, the first two terms of Eq. 2 have to be combined because the diffuse fraction cannot be separated from the total radiation. For measuring the diffuse part of the radiation directly a second pyranometer would be necessary. The first term in the modified output energy equation (Eq. 4) refers thus to the total irradiance G_{tot}. The zero-loss efficiency $F'(\tau\alpha)_{en}$ and incidence angle modifier K_θ need to be found for the total irradiance.

Due to the lack of wind speed data the equations' terms that include the wind speed u have to be treated with caution. To be able to evaluate the influence of the wind speed the following approach is suggested: The calculation with Eq. 4 is done without the wind speed terms, and for the calculation with Eq. 5 a constant wind speed of 3 m/s is assumed. The values of both calculations are to be compared in order to determine the influence of the wind speed.

As the long-wave irradiance is not measured in this setup, this term is not taken into consideration. Apart from that it was very difficult to calculate the zero-loss efficiency $F'(\tau\alpha)_{en}$ and incidence angle modifier K_θ seperately because no measurements for the collector in horizontal position exist. Furthermore, there is no data taken explicity for a situation where $T_a = T_m$, so $F'(\tau\alpha)_{en}K_\theta$ shall be calculated via multiple linear regression together with the other variables, and the zero-loss efficiency and incidence angle modifier shall not be calculated seperately.

The values from the collectors' specifications, obtained in a test laboratory, are $F'(\tau\alpha)_{en} = \eta_0$=0,811 and $K_\theta(\theta = 50°) = 0{,}98$ for the Savosolar collector, and η_0=0,781 for the KBB collector. The incidence angle modifier for the KBB collector is not known; in case an assumption has to be made for it, the value from Savosolar's collector shall be used. Then the values for $F'(\tau\alpha)_{en}K_\theta$ are 0,795 for the Savosolar collector, and 0,765 for the KBB collector, respectively.

For the left hand side of Eq. 4 and 5 the instantaneous heating power is calculated using the formula [4, Chap. 6]

$$\dot{Q}_{inst} = \dot{m}C_{\text{tyfo}}(T_{out} - T_{in}). \tag{6}$$

Here $\dot{m}$ stands for the mass flow, which is determined by multiplying the volume flow q (about 70 l/h, as already mentioned) and the density of the Tyfocor-solution ρ_{tyfo} as follows: $\dot{m} = \dot{q} \cdot \rho_{\text{tyfo}}$. The specific heat capacity of the Tyfocor-solution at T_m is called C_{tyfo}, and its values can be found from the technical specifications [16]. In order to simplify the calculation procedure, functions for specific heat capacity vs. temperature and density vs. temperature are fitted, based on the concentrations found for both collector cycles. The linear fit functions for the concentrations at hand are listed in Tab. 6, their plots are shown in Figs. 10 and 11.

Table 6: Linear fit functions for density ρ_{tyfo} and specific heat capacity C_{tyfo} vs temperature T, found for two different Tyfocor concentrations

	Savosolar (concentration 34%)	KBB (concentration 44%)
C_{tyfo} / kJ/kg·K	= 0,0033 $\cdot T$ + 3,7133	= 0,0040 $\cdot T$ + 3,5200
ρ_{tyfo} / m^3/kg	= -0,63 $\cdot T$ + 1046,58	= -0,78 $\cdot T$ + 1061,53

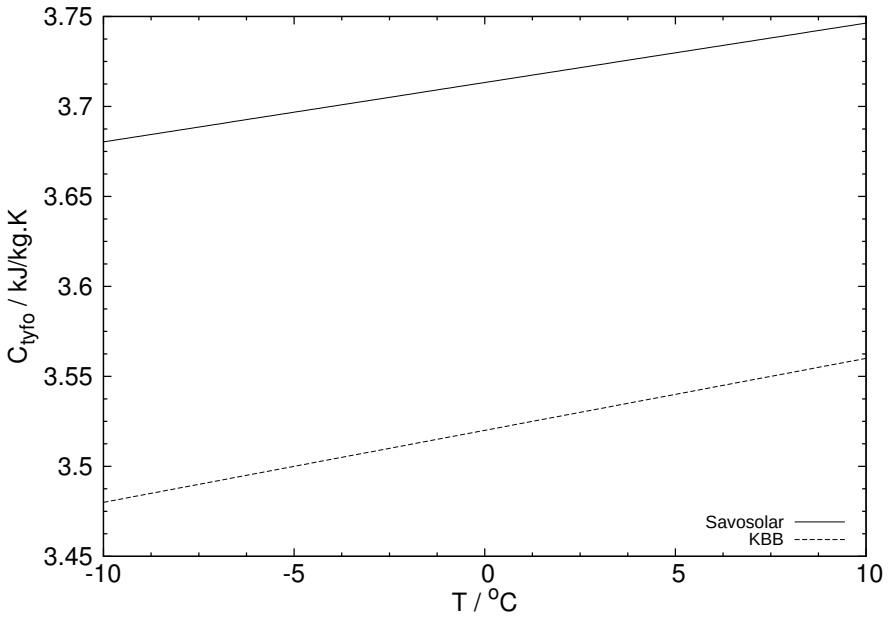

Figure 10: Fit function for the specific heat capacity C_{tyfo} vs temperature T

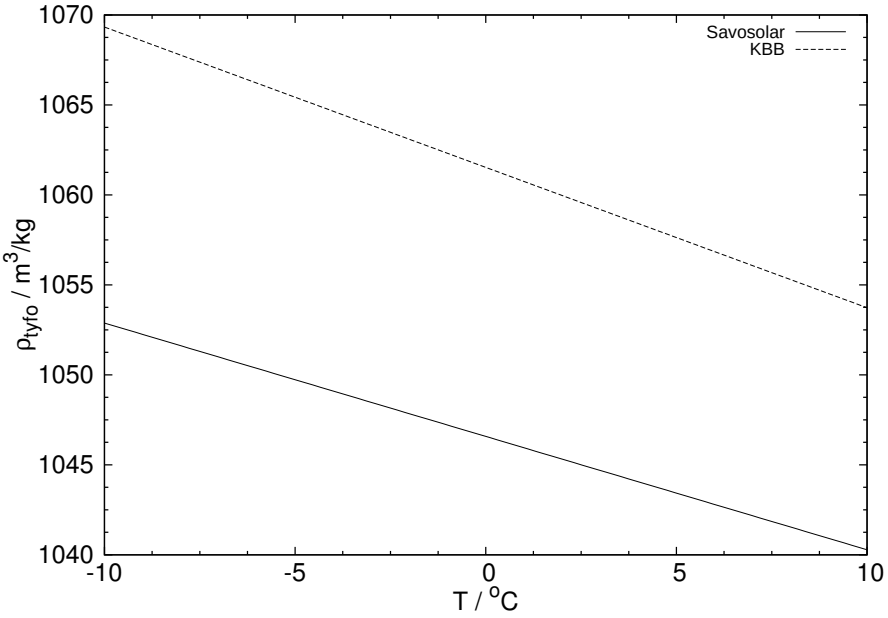

Figure 11: Fit function for the fluid density ρ_{tyfo} vs temperature T

3.3 Measurement system for microclimate testing

Finding out about possible condensation on the inside of the collector glazing was one of Savosolar's aims for this project. In this section an experimental setup for measuring the collector's microclimate with respect to condensate formation is described. The conditions inside and outside the collector, as well as the monitoring of occuring condensation were used to determine whether a certain ventilation solution works or not. A rough sketch of the setup is shown in Fig. 12. A detailed drawing of the components underneath the shading plate can be found in Fig. 13, and a photograph of the shading plate in Fig. 14. In the initial ventilation setup a diagonal ventilation method was used, as described in section 2.2. In order to collect the data all compontents of the setup were connected to a PC.

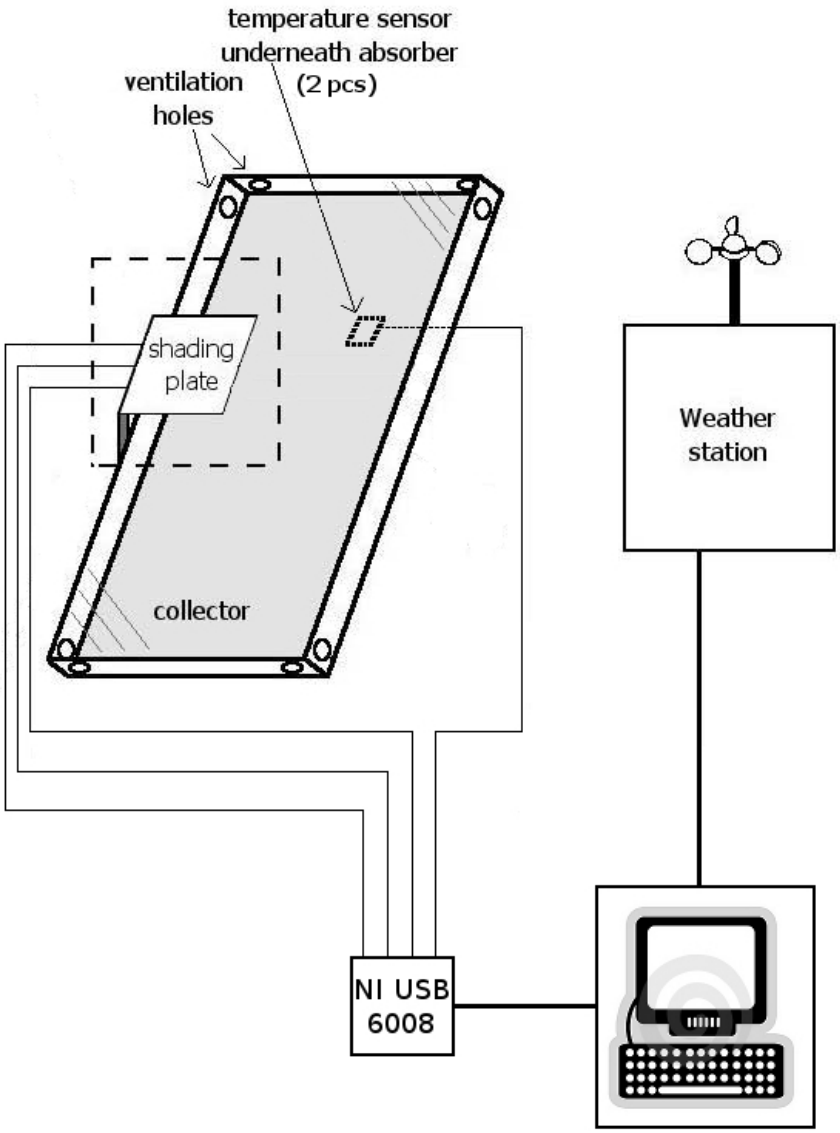

Figure 12: Experimental setup for microclimate measurements; the two absorber sensors were positioned on the left and right of the absorber's back side; all sensors were situated at about halfway of the absorbers height

Ambient conditions

The interesting ambient conditions that were measured are temperature, pressure, relative humidity and wind speed. A comprehensive weather station performed these measurements. The model chosen was the WS2801 weather station by Lacrosse Technology. In addition to the already mentioned parameters it also measured the amount of rain, which in our case is of no interest. The accuracies for the different sensors are listed in Tab. 7. They can be found

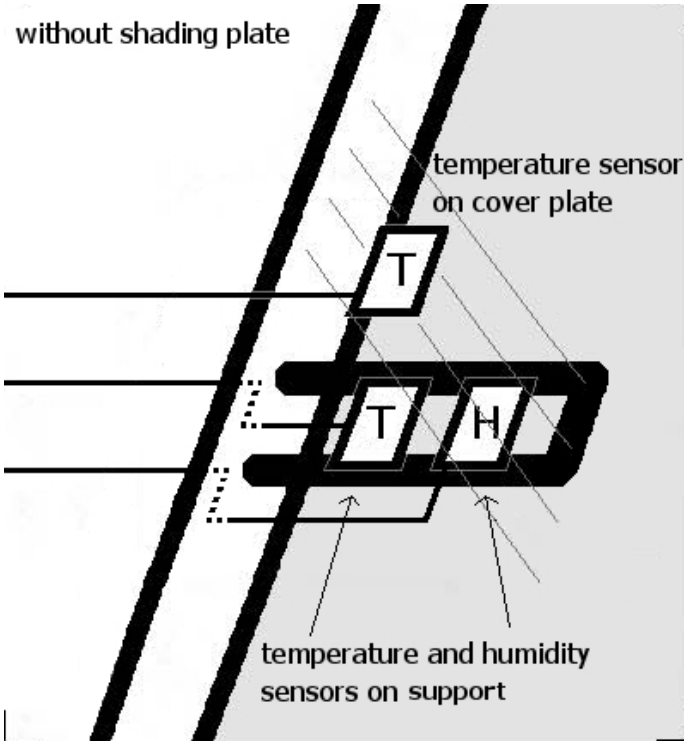

Figure 13: Detailed schematics of area underneath shading plate; the shading plate was mounted such that it did not touch the cover plate, and the support ensured that the sensors inside the air gap touched neither cover nor absorber plate

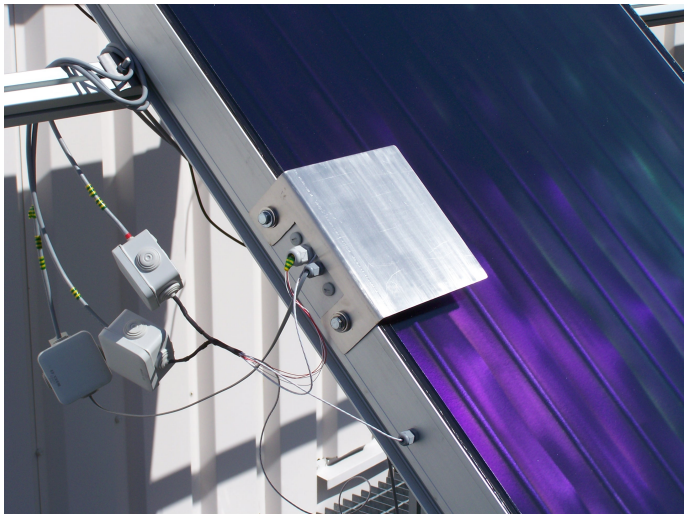

Figure 14: A photograph of the shading plate mounted on the collector's side

from the product's user manual. Unfortunately the wind sensor delivered with the station did not work, and replacement did not arrive before the end of the measurement period, so no wind data is available.

Temperature

The temperature inside the collector was measured at four positions: On the left and on the right side of the back of the absorber, inside the air gap, and on the cover plate (see also Figs. 12 and 13). That way a comprehensive monitoring of the collector's temperature behaviour could be ensured. For measuring the temperature 4-wire Pt100-sensors are used, which need to be supplied with a constant current during the measurements. A constant current source connected to all temperature sensors was constructed by the Physics Department workshop for this purpose. The Pt100 sensor model was chosen because the sensors that were already included in the thermal performance measurement setup were also Pt100 sensors. The behaviour of all temperature sensors was thus expected to be similar.

The temperature sensors for the absorber are SA2C-RTD surface sensors by the company Omega. They are class A Pt100-sensors, and their accuracy is specified as ± 0,15 °C + 0,002 $\cdot T$, where T is the measured temperature. They have a self-adhesive surface, so no glue was necessary to attach them. To ensure that no direct sunlight influenced the measurements they were mounted in between absorber and insulation.

The temperature sensor for the cover is of the same type as the absorber sensors. Here the direct sunlight might falsify the measurements considerably, so a shading plate was mounted on the side of the collector (*cf.* Fig. 14). The shading device did not touch the cover directly, as it might have influenced the cover temperature locally. It was assumed that the temperature difference between shaded and unshaded parts of the cover plate are not substantial, *i.e.*, that the influence of the shade is negligible.

The temperature inside the air gap was measured using the class A sensor 010010TD of the company Labfacility, with the already mentioned accuracy for its class of ± 0,15 °C + 0,002 $\cdot T$. It was fastened on a support inside the collector and situated directly underneath the shading plate to avoid direct sunlight (*cf.* Fig. 13). The support was mounted such that the sensor did not touch absorber or cover plate directly.

Pressure

The pressure difference between inside and outside the collector is of the order of 1 Pa [12, Chap. 5.2]. An instrument with this precision was not available at a reasonable price and size for this setup; differential pressure meters were not suitable because they disturb the free air flow. Therefore, the pressure measurement inside the collector was neglected and the outside pressure values were used. This is a reasonable approximation, since at an outside pressure of 101,325 kPa the error due to a 1 Pa difference would be about 0,001 %.

Relative humidity

A humidity sensor was placed inside the collector's air gap, on the same support as the inside temperature sensor (*cf.* Fig. 13). Also here avoiding direct sunlight was important, which was ensured by the support being underneath the shade. The accuracy of the sensor is given as ± 3,5 % relative humidity. A constant voltage was supplied for running the sensor. The voltage was provided by the National Instruments datalogging device. More information on the device can be found in the later following paragraph "Data acquisition".

Solar irradiance

A pyranometer was added to the setup, mainly for the purposes of the thermal performance measurements mentioned earlier. However, its data was collected via the microclimate setup. A summary of all used sensors and their accuracies can be found in Tab. 7.

Condensation

In addition to the measurements of the collector's microclimate it is very important to know during which periods and at what conditions visible condensation actually takes place. For that purpose a webcam was used to take pictures of the cover plate in regular intervals. Only the occurence (and not the amount) of condensation was of interest at this point. As outdoor webcams seemed too expensive for the purposes of this study, a weatherproof construction was improvised using a small indoor webcam and placing it inside the casing of an outdoor halogen lamp. Pictures of assembly and placement in front of the collector are shown in Fig. 15 and Fig. 16. The construction worked reliably and was found to be weatherproof. Due

Table 7: Sensors used in microclimate test setup; accuracies taken from the sensors' specifications

measured parameter	sensor name	accuracy
absorber temperature (2x)	Omega SA2C-RTD	± 0,15 °C + 0,002 $\cdot T$
cover temperature	Omega SA2C-RTD	± 0,15 °C + 0,002 $\cdot T$
air gap temperature	Labfacility 010010TD	± 0,15 °C + 0,002 $\cdot T$
air gap relative humidity	Honeywell HIH-4000-001	± 3,5 % relative humidity
pyranometer	Kipp&Zonen CM 11	± 10 W/m^2
WEATHER STATION		
ambient temperature	WS2801	± 0,1 °C
ambient pressure	WS2801	not stated in specs
ambient relative humidity	WS2801	± 1 % relative humidity
wind speed	WS2801	± 0,1 m/s, but sensor N.A.

to the limited placement possibilities the webcam had to be attached to the railing in front of the collector. This means that only parts of the collector could be captured; thus it was decided that the camera was to be directed on the collector's lower part, where condensation is more likely to occur. The webcam was connected to the measurement PC and controlled by a program which took a picture every 15 minutes. These pictures (see example in Fig. 17) were saved for further examination.

Data acquisition

The weather station and the webcam were directly connected to the measurement PC. The collector sensors and the pyranometer were connected to a datalogging device by National Instruments (model NI USB-6008), which itself was connected to the PC. The sensor signals were processed by the device and sent to the computer. A computer program was created which displayed the momentary parameter values and wrote an output file for the averaged values for every minute of the measurement. The program was built using the National Instruments LabVIEW software, which is a widely used tool for datalogging and process control in laboratory scale. Fig. 18 shows a picture of the program's user interface.

Figure 15: A photograph of the webcam inside the open halogen lamp casing

Figure 16: A photograph of the webcam in its final position on the railing in front of the collector; the cam is directed at the lower part of the collector

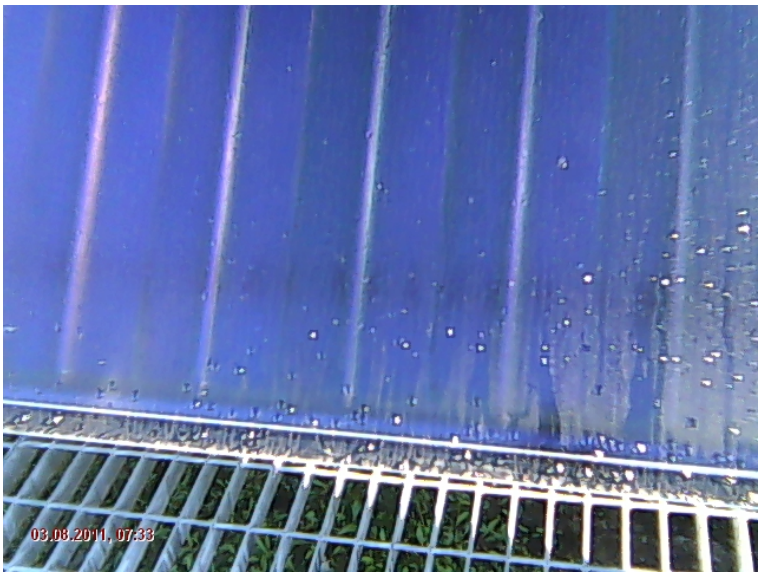

Figure 17: An example picture taken by the webcam on 03.08.2011, with morning dew condensated on the outside of the cover plate

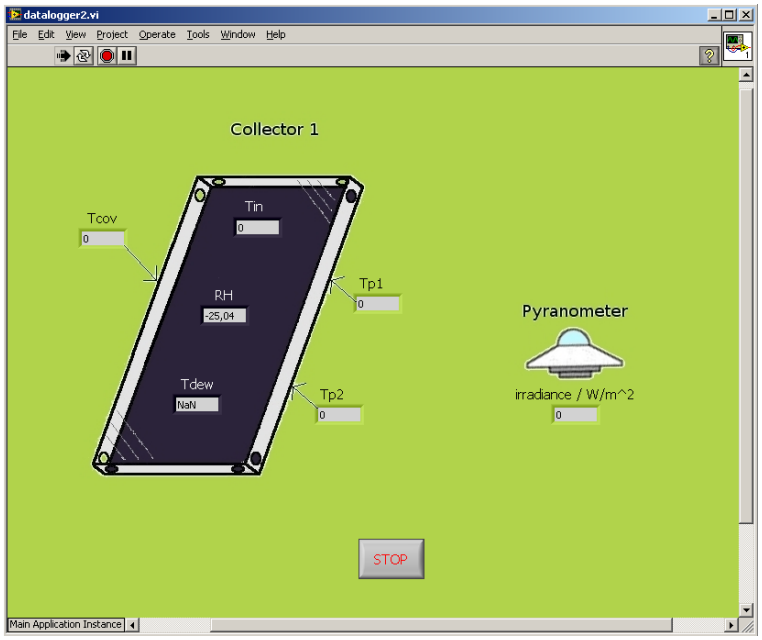

Figure 18: The user interface of the condensation setup datalogger; all measured parameters' momentary values can be observed. The screenshot was taken without the setup being attached, so the displayed values are not typical for the measurements. The arrows of the absorber plate temperatures "Tp1" and "Tp2" point only roughly to the absorber and no exact position is aimed at. As mentioned before, these two sensors are situated on the left and on the right side of the back of the absorber plate.

4 Data selection and calculations

4.1 Thermal performance measurements

The data selection for the thermal performance analysis is based on the pyranometer data. The irradiance is plotted against time, and from these plots "clear sky" days are identified. A clear sky day, meaning a sunny day without cloud cover, has a charateristic curve like the one from Karlsruhe, 2.7.1991, shown in Fig. 19. The irradiance increases until a maximum during solar noon and then decreases again. The curve is approximately symmetric with the symmetry axis located at solar noon.

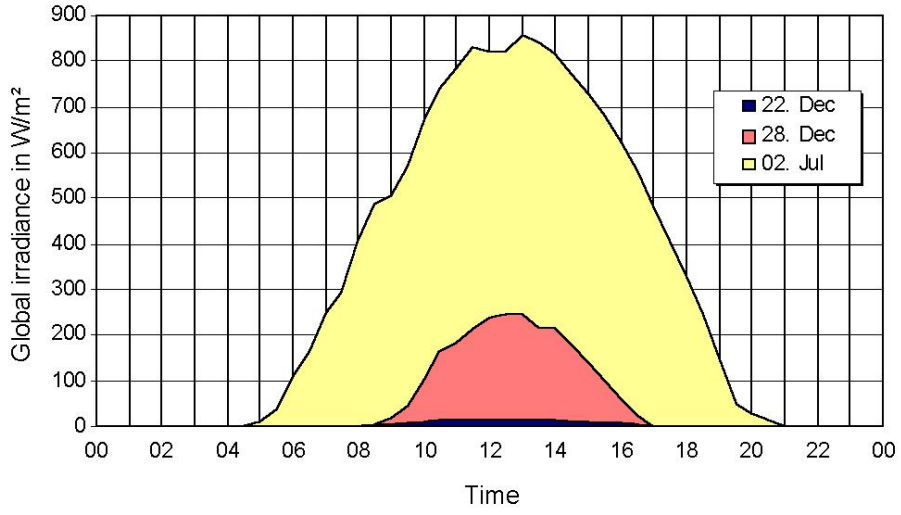

Figure 19: A plot of global irradiance vs. time in hours for three days in Karlsruhe during the year 1991; the 2nd of July is a good example of a clear sky day, with a smooth intensity curve [2]

After the clear sky days are identified, T_m and dT_m/dt and $\dot{Q}_{inst}$ are calculated for them. All missing parameters are calculated with and without wind influence. The calculation method is called multiple linear regression and it can be performed *e.g.* using spreadsheet software. In this method the data is fitted with an equation of the form

$$y = b_1 \cdot x_1 + b_2 \cdot x_2 + ... + b_n \cdot x_n, \tag{7}$$

where $x_1 ... x_n$ and y represent different data sets, and the coefficients $b_1 ... b_n$ are found through fitting. In our case, $y \equiv \dot{Q}_{inst}$ and the x-values are assigned to the measured values on the right hand side of Eqs. 4 and 5.

A summary of the data handling procedure looks as follows:

1. Identify clear days using pyranometer data
2. Calculate T_m and dT_m/dt and $\dot{Q}_{inst}$ using the available clear sky data
3. Find all missing parameters for Eq. 5 using the available clear sky data (at times when $G_{tot} > 700$ W/m^2)
4. Find all missing parameters for Eq. 4 using the available clear sky data (at times when $G_{tot} > 700$ W/m^2)

Comparison of pyranometer and sensor CS10

An important aspect of the data analysis in this thesis is the comparison of the pyranometer data with the data taken from sensor CS10. Measuring the solar irradiance is a very crucial part of the method. As the pyranometer is temporarily included in the setup, it was checked that the sensor CS10 is producing reliable results.

Comparison of Savosolar and KBB collector

The analysis procedure described above is also applied to the data from the KBB collector to enable a comparison between Savosolar's and KBB's collectors. The final results for the thermal performance analysis for both collectors shall be compared and evaluated.

Time constant measurements

Time constant measurements for the collectors were not conducted during this measurement period.

4.2 Microclimate measurements

In order to find out when and under which conditions condensation occurs on the inside of the cover plate, the webcam pictures are examined for traces of condensation. Data from days during which condensation occured is then handled in more detail. It is also checked, whether the relative humidity inside the collector $\omega_{rel,in}$ is ever higher than the ambient relative humidity $\omega_{rel,amb}$, and whether the dew-point temperature inside the collector T_{dew} is ever

higher than the cover temperature T_c. These two conditions indicate, if the circumstances are favourable for condensation to form on the cover plate.

After the relevant data has been selected, it is evaluated what conditions influence the condensation behaviour most, and how often and how long condensation occurs. From the results conclusions can be drawn on how much of a problem condensation poses, and how well suited the diagonal ventilation option is for Savosolar's collector. A summary of the steps to analyze the microclimate data looks as follows:

1. Search pictures for evidence of condensation
2. Check data for situations when $\omega_{rel,in} \geq \omega_{rel,amb}$ and/or $T_{dew} \geq T_c$
3. Determine frequency and duration of condensation cases
4. Evaluate gravity of problem, and assess ventilation solution

5 Results

The measurement period was started on 29.6.2011 with the installation of the microclimate setup and its software. The RESOL system had been collection data already earlier, but for this thesis the daily files were gathered starting from 29.6.2011. The pyranometer was added to the setup later, on 15.7.2011. The measurement period was ended on 14.9.2011 due to a collector being replaced on the test site. Complete data sets consisting of all planned measurements and data taken for every minute of the day are available from 16.7.2011 to 8.9.2011, in total 55 days.

5.1 Thermal performance tests

The very first step for finding out about the thermal performance of the Savosolar and KBB collectors was to search the data for clear-sky days. From the pyranometer data these were found to be 22.7. (although the weather data is almost completely missing for this day), 31.7., 3.8., 4.8., 27.8., 28.8., 4.9. and 6.9.2011. However, most of these days do not have a completely smooth irradiation curve, indicating some cloud cover was probably present during parts of the days. The plots shown in this section are from 3.8.2011, which was closest to a perfect clear sky day (*cf.* Fig. 19). In appendix B the respective plots for the other days can be found (not included in the public version of this thesis).

For the mentioned days the Savosolar and KBB collectors' RESOL data, the condensation setup data and the weather station data was collected to one spreadsheet file per day and averaged in ten minute intervals. The temperature sensors S12 of both Savosolar and KBB collector were initially used for measuring the ambient temperature, but on 26.8.2011 they were attached to the collectors' backsides. In the KBB collector's setup an additional temperature sensor (S18) was used for measuring the inside of the collector casing at a place between insulation and back wall. On sunny days all ambient temperature sensors measured temperatures higher than the data from the Finnish Meteorological Institute (FMI) indicates. This leads to the conclusion that none of the ambient temperature sensors were placed properly, *i.e.* in the shade. The sensors placed behind the collectors were probably influenced considerably by the collectors back losses.

The data for the flow meters IMP1a and IMP1b consists only of zero values. The reason

for this is that the flow in both primary cycles is too low for the flow meters to measure. As stated earlier, a value of 70 l/h was proposed for the flow inside the primary cycles, and from the pump values for R1a and R1b one can deduce whether liquid was circulating or not. The data for the secondary fluid cycle and air heater pumps R2 and R3 is available in the RESOL file for the Savosolar collector. According to the pump data, both pumps work between 19:00 and 04:30. The flow meter data however only shows values different from zero in the start-up phase around 19:00. After 1,5 - 2 hours the flow values again go down to zero. A probable explanation for this is that the flow peaks at the start-up and then slowly settles to a steady flow rate. A flaw in the control unit leads to the unit not registering those flow values anymore, as the change in flow is too small.

The pyranometer data shows an unusual curve in clear sky conditions, see Fig. 20. Instead of being round and smooth (*cf.* Fig. 19) the irradiation values increase rather fast and then form a plateau around solar noon.

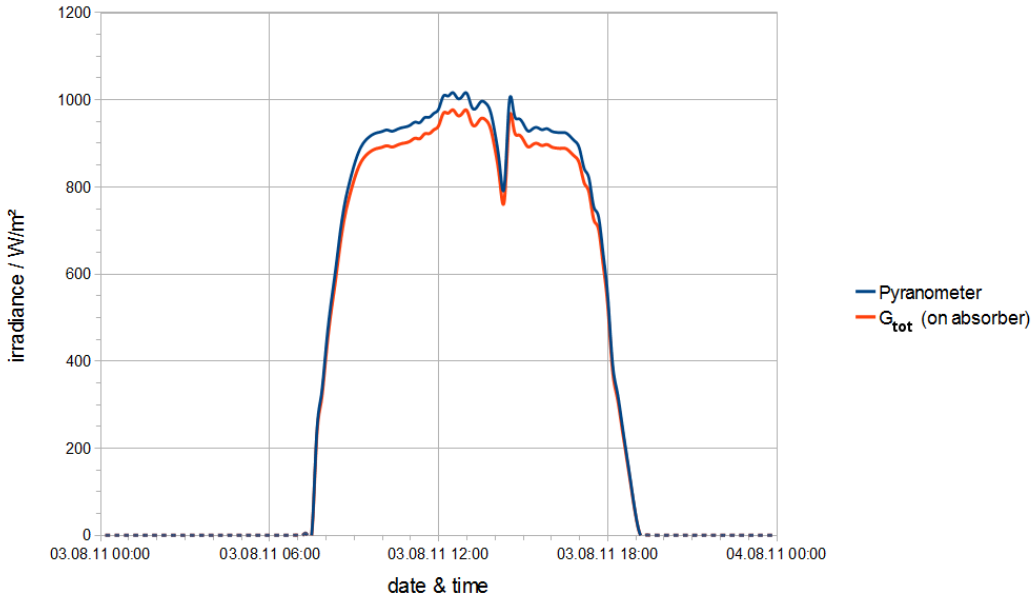

Figure 20: The pyranometer data and the calculated data for G_{tot}, taking into account the absorptance of the glass cover, for 03.08.2011; note the plateau-shaped curve.

An explanation for this might be the white factory wall, which is responsible for a lot of reflected radiation that influences the pyranometer measurement. This explanation could be checked by installing a second pyranometer for which the direct beam radiation is blocked, resulting in a measurement of only the diffuse part of the incoming radiation. In Fig. 20 also

the calculated data for G_{tot} is displayed. It is calculated from the pyranometer values G_{pyr} and the transmittance of the glass covers: $G_{tot} = 0,92 \cdot G_{pyr}$.

5.1.1 Calculation of parameter values

In the spreadsheet files for each day the following parameters were calculated:

- $T_m = (T_{out} - T_{in})/2$
- dT_m/dt via taking the difference between two subsequent values for T_m and dividing it by 600 seconds (= 10 minutes)
- $T_m - T_a$
- $(T_m - T_a)/G_{tot}$
- ρ_{tyfo} and C_{tyfo} for both collectors according to the fit equations in Tab. 6
- $\dot{Q}_{inst}$ according to Eq. 6, and $\dot{Q}_{inst}/A_a$
- $\eta = \dot{Q}_{inst}/(A_a \cdot G_{tot})$, *i.e.* the instantaneous efficiency

The output power $\dot{Q}_{inst}$ is only calculated for the primary cycle pump R1a/R1b being switched on, otherwise the value is set to zero. The flow value used is weighted with the fraction of full pump power in %. Thus the formula for the flow value changes slightly to become $\dot{q} = z\ \%/100\% \cdot 70$ l/h, with z being here the percentage of full pump power.

Negative irradiance values recorded by the pyranometer are set to zero. The reason for negative values being measured is probably a certain offset induced by the data acquisition system.

5.1.2 Ambient temperature

There are in total seven ambient temperature sensors in the setup, plots for their measurements on 3.8.2011 can be found in Fig. 21. All sensors' measurements are in good agreement, and considering the rather high measured temperatures (as mentioned before), probably all of them (including the sensor belonging to the weather station) were placed so that they were influenced by direct sunlight. For the calculations the average value for all measurement was taken.

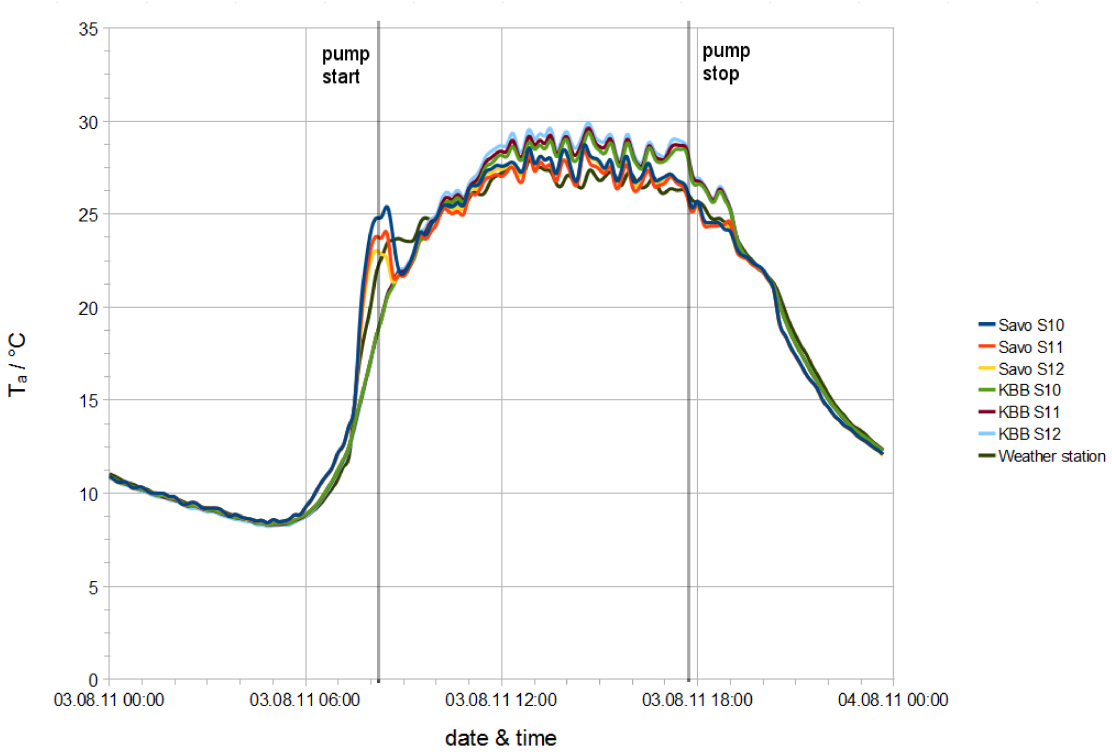

Figure 21: The ambient temperature data for all ambient temperature sensors on 03.08.2011; the sensors are very much in agreement with each other.

5.1.3 Absorber plate and fluid inlet and outlet temperatures

In Fig. 22 the measured data of the three absorber plate temperature sensors and the fluid inlet and outlet sensors of the Savosolar collector is displayed. The absorber temperature was measured at three different points: close to the fluid outlet (”Savo S1”), and in the center of the collector (vertical direction) on the fluid inlet (”Cond 1”) and on the fluid outlet side (”Cond 2”; see Fig. 8 for the U-shaped tubing pattern). The curve shapes are in good agreement with each other. The sensor from the Savosolar collector’s RESOL setup (”Savo S1”), positioned close to the outlet, shows the lowest temperatures. This is probably due to the fact that the sensor ”Savo S1” is not as closely attached to the absorber as the sensors ”Cond 1” and ”Cond 2”. Furthermore, its position is very close to the edge of the absorber, whereas the sensors ”Cond 1” and ”Cond 2” are placed in rather central positions. The inlet side sensor of the condensation setup ”Cond 1” shows slightly higher values than the sensor ”Savo S1”, and the outlet side sensor ”Cond 2” shows the highest values. There is one exception to this between 06:00 and 08:00 a.m., where the inlet side sensor ”Cond 1” shows higher values than the outlet

side sensor "Cond 2". A possible explanation for this behaviour is that in the early morning the outlet side of the collector is still shaded by the collector frame, whereas the inlet side is already completely exposed to the incoming solar radiation.

The outlet temperature T_{out} and the plate temperature measured by sensor "Savo S1" are almost identical because they are positioned very close to each other. The inlet temperature rises steadily after the primary cycle pump is turned on, as the fluid in the storage tank heats up, but stays still well below the outlet temperature. After the pump is shut down the temperature still rises for a while due to the stagnation in fluid flow. After that it sinks and the shape of the inlet temperature curve fits the shape of the other curves.

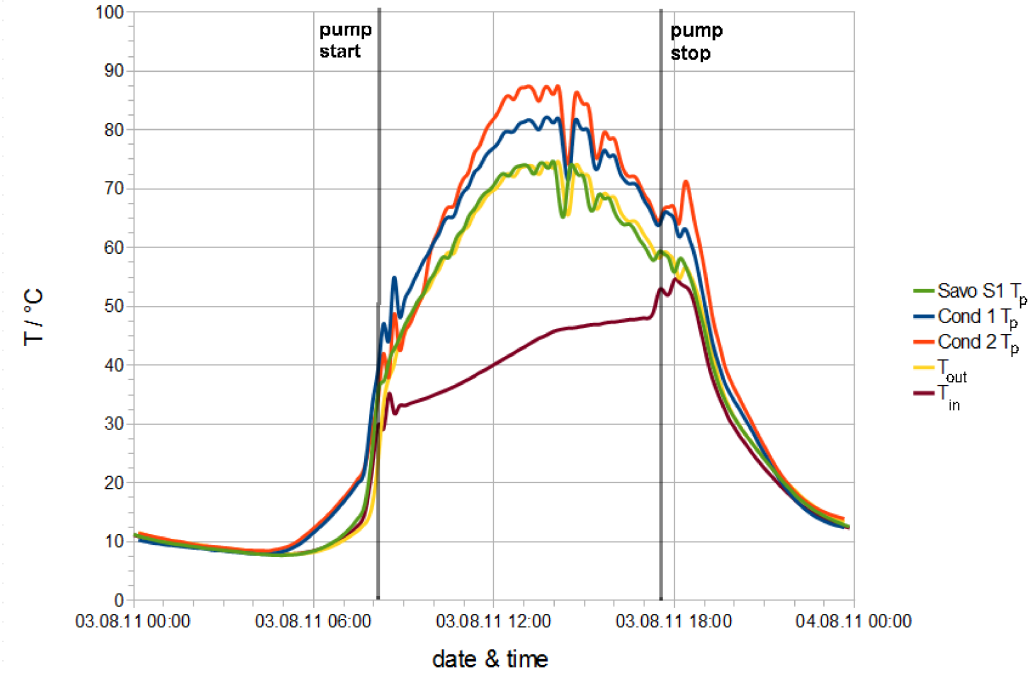

Figure 22: The absorber plate temperature data for all absorber plate temperature sensors (one from the RESOL setup and two from the condensation setup) and for inlet and outlet temperatures on 03.08.2011; the measured absorber temperatures differ according to the sensors' placements on the absorber, but the general shapes of these three curves are in good agreement. The outlet temperature curve matches the curve "Savo S1" rather well as they are positioned close to each other. The inlet temperature rises steadily during the day, with a slight peak after the primary cycle pump is shut down.

5.1.4 Instantaneous efficiency values

Calculating the instantaneous efficiency values η produced quite remarkable results. In many cases the efficiency is greater than 1 (or 100%), because the calculated output power was higher than the incoming radiation. As this result is not in agreement with the laws of physics, the most probable explanation is that the proposed flow rate value of 70 l/h must be wrong. This is also supported by the fact that the flow meter should actually be able to measure a flow rate of 70 l/h, however the measured values are all zero, indicating a too low flow rate for the device. Another influencing factor might be that the space around the collectors was heated up due to the presence of the factory wall.

Due to the aforementioned circumstances, and due to the fact that no measurements for several different stable $T_m - T_a$-values could be taken, efficiency curves for the collectors cannot be determined with the setup at hand. To illustrate this the efficiency curve for the Savosolar collector found from the available data of the thermal performance setup is shown in Fig. 23. For comparison, a curve for the same collector measured under controlled circumstances in a test laboratory is shown in Fig. 24. It is evident that the curve obtained from the thermal efficiency setup does not give any sensible information.

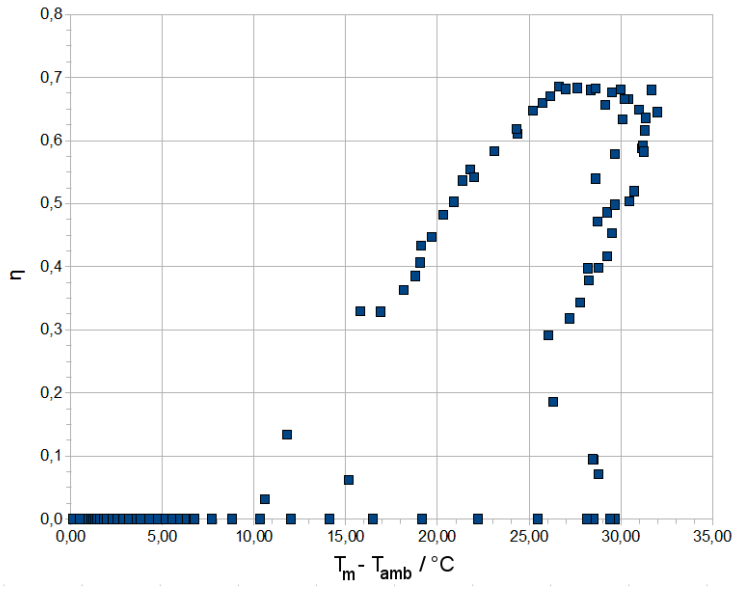

Figure 23: Efficiency curve for the Savosolar collector obtained from the thermal performance measurement setup

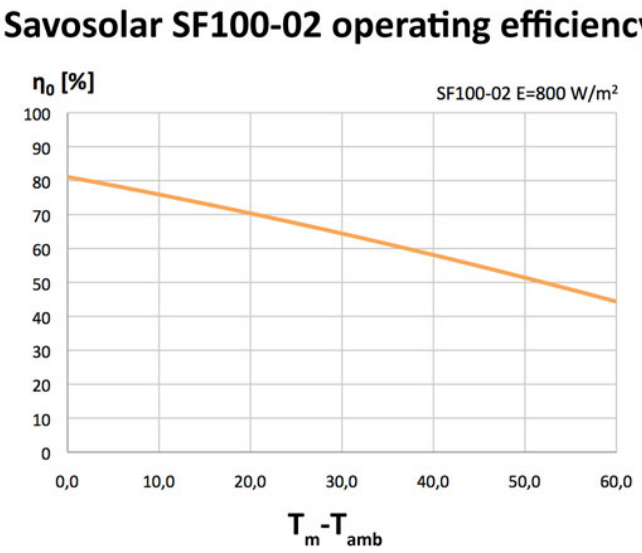

Figure 24: Efficiency curve for the Savosolar collector obtained in a test laboratory; picture taken from Savosolar's homepage [3]

5.1.5 Finding the coefficients via multiple linear regression

The coefficients of Eq. 4 and 5 were calculated via multiple linear regression, and only using data where $G_{tot} > 700$ W/m^2. The results are quite unsatisfying, as in some cases zero loss efficiencies far greater than 1 (or 100 %) are found (see also paragraph before). For the other coefficients the results produce odd values as well. Obviously the data sets available are not fitting to the purpose, due to the less than ideal test circumstances, *e.g.* no stable fluid inlet temperatures. The multiple linear regression method was used as it would be for actual testing.

5.1.6 Comparison of pyranometer and CS10 sensors

When comparing the pyranometer data with the data measured by the two CS10 sensors, the most striking difference is the pyranometer's much higher sensitivity to diffuse radiation. The CS10 sensors are due to their construction and their casing basically only sensitive to direct (or beam) radiation, which results in a rather late, but very steep increase in irradiance, and a corresponding steep decrease. Around solar noon the values for both CS10 sensors seem to stagnate, which is due to the solar irradiation exceeding the measuring range of the RESOL unit. Their measured irradiance values around solar noon tend to be higher than the

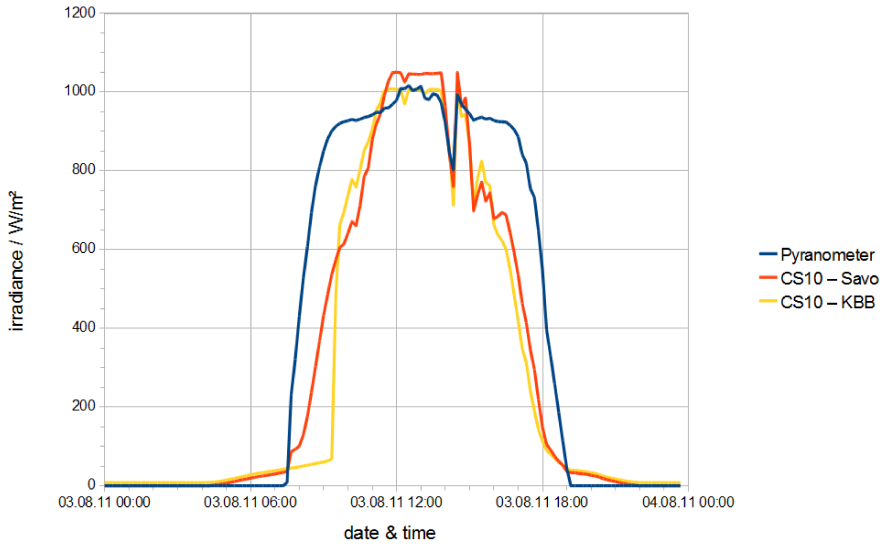

Figure 25: Irradiation data measured with the pyranometer and both CS10-sensors on 03.08.2011; the pyranometer's higher sensitivity to diffuse radiation can clearly be seen in the much earlier increase and much later decrease in radiation, and both CS10 sensors' measuring range seems to be exceeded around solar noon, judging from the almost unchanged irradiance values.

pyranometer values (see Fig. 25 for the plot).

5.1.7 Comparison between Savosolar and KBB collector

As stated before, actual efficiency values could not be obtained from this setup. However, the power output of the Savosolar and the KBB collector was qualitatively compared. From Fig. 26 the power output on 3.8.2011 for both collectors can be compared, based on the assumed flow rate of 70 l/h.

Another indicator for the collectors' output is the energy stored in their storage tanks over one day. Thus, the top and bottom temperatures in the morning (before primary cycle pumps were switched on, here called *initial state*) and evening (after the primary cycle pumps were switched off, but before the secondary cycle pump was switched on, here called *final state*) are compared. The initial and final state correspond to the lowest and highest temperatures of the storage tanks during that day. Because of a considerable stratification especially during the morning hours the tank is split into nodes, and the temperature in each node is calculated for initial and final state. A linear temperature gradient in the tanks is assumed. With the temperature differences for each node n the energy stored in each node after the day in

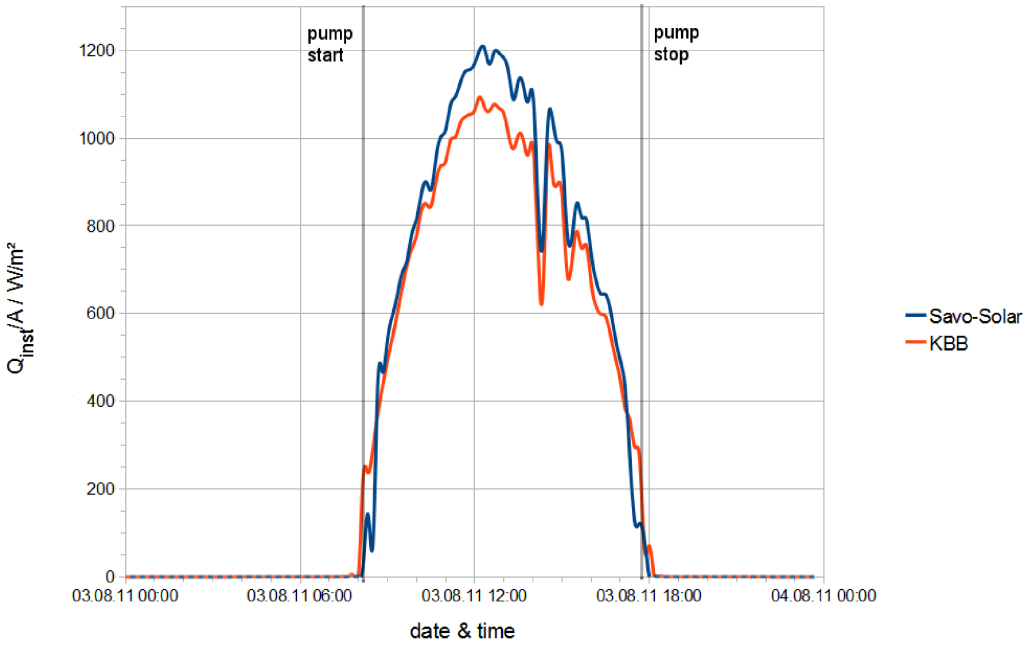

Figure 26: Power output for the Savosolar and KBB collector on 03.08.2011 based on a flow rate of 70 l/h for both collectors; the Savosolar collector gives a higher output.

question can be calculated using the following equation:

$$\Delta U_n = \frac{1}{n} m_w \cdot C_w \cdot (T_{n,f} - T_{n,i}). \tag{8}$$

Here m_w stands for the mass of water, calculated via the tank capacity of 330 l and a density of water $\rho_w = 997,04$ kg/m^3. $C_w = 4{,}18$ kJ/(kg·K) is the heat capacity of water, and $T_{n,f}$ and $T_{n,i}$ stand for the final and inital state temperatures of the respective node n. Then the energies calculated for each node are summed up to give the total energy stored in the tank during the day of interest.

For the actual calculations six nodes were used. Tab. 8 shows the results for the energy stored in both colletors' storage tanks during 3.8.2011. Surprisingly, the KBB collector tank stores more energy than the Savosolar collector, although the instantaneous collector output is considerably lower for the KBB collector. The most probable explanation for this is again connected to the flow rate problem that was already faced: not only do the flow rates in the primary cycles differ from the assumed 70 l/h-value, they are probably not the same. Another influencing factor is that in general the primary cycle pump of the KBB collector was running slightly longer than the Savosolar collector pump. For this day (and most other test days) the difference is however only ten minutes (Savosolar pump running time: 9h 40min, KBB pump

Table 8: Stored energies during 3.8.2011 in storage tanks for Savosolar and KBB collector

Collector	energy stored during 3.8.11
Savosolar	5,65 kWh
KBB	5,88 kWh

running time: 9h 50min), which is rather short and probably not the only reason why more energy is accumulated by the KBB collector. The values for all clear sky days can be found in appendix A (not included in the public version of this thesis).

In order to get an estimate for both collectors' primary cycle flow rates some "reverse engineering" is applied: The efficiency curves from the collector specifications, and the values for $T_m - T_a$ and G_{tot} are used in order to find out the collectors' efficiencies η_{spec} according to the equation [8]

$$\eta_{\text{spec}} = \eta_{\text{spec},0} - a_1 \cdot \frac{T_m - T_a}{G_{tot}} - a_2 \cdot \left(\frac{T_m - T_a}{G_{tot}}\right)^2. \tag{9}$$

The values for $\eta_{\text{spec},0}$, a_1 and a_2 are taken from the collector specifications [14, 15]. By multiplying η_{spec} and G_{tot} the expected output power per square meter of collector area $\dot{Q}_{exp}/A_a$ is found. Now this expected value and the actual value $\dot{Q}_{inst}/A_a$ are compared. If we assume all other factors in the equation for $\dot{Q}_{inst}/A_a$ to be constant, the actual flow rate $\dot{q}_{act}$ is found via

$$\dot{q}_{act} = \frac{\dot{Q}_{exp}/A_a}{\dot{Q}_{inst}/A_a} \cdot 70\frac{\text{l}}{\text{h}}. \tag{10}$$

After conducting these calculations a rough estimate for q_{act} would be 40 l/h for the Savosolar collector, and 45 l/h for the KBB collector. The power output plot from Fig. 26 then changes considerably, see Fig. 27 for a new version. In this case, the KBB collector gives a slightly higher output.

The results found using the new flow rates are by no means suitable for any kind of comparison because they were found via "reverse engineering" and not directly from measurements. Their purpose is mainly to explain why there is more stored energy in the KBB collector's storage tank. In this case the actual power output from the KBB collector seems to be higher than from the Savosolar collector, which is in agreement with the storage tank calculations.

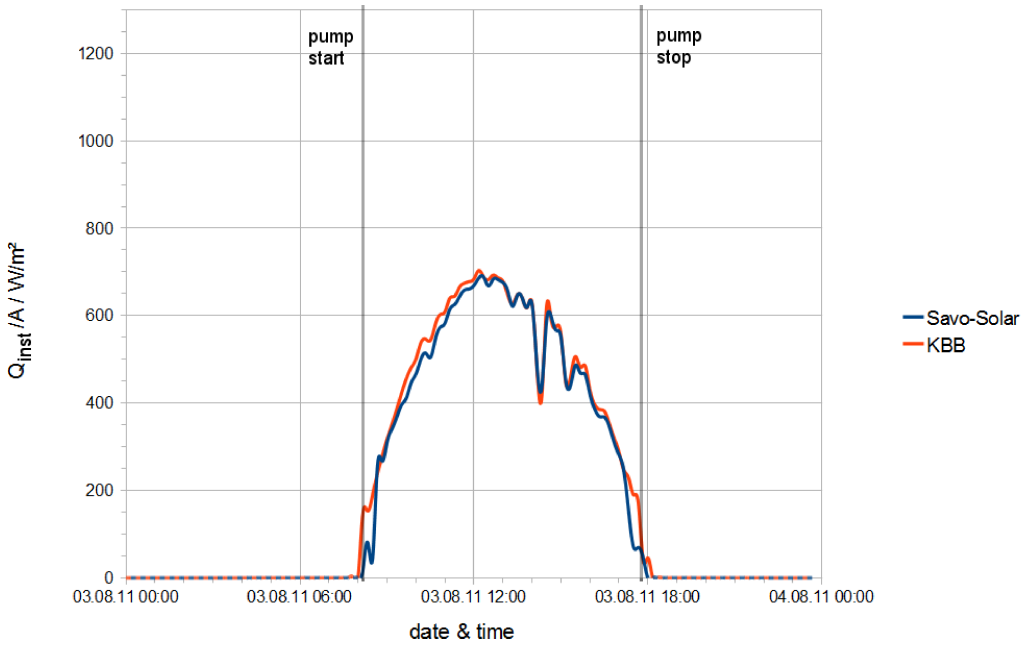

Figure 27: Power output for the Savosolar and KBB collector on 03.08.2011 based on the new flow rates of 40 l/h for the Savosolar and 45 l/h for the KBB collector; the KBB collector gives now a slightly higher output.

For some other measurement days this does not necessarily hold true, however the new values for the flow rates bring a large error into the calculations.

If anything, the findings from this section show how very important it is to have accurate flow rate measurements, or else even a comparison of two collectors in otherwise almost identical setups cannot be conducted.

5.2 Microclimate tests

The webcam pictures of the Savosolar collector were searched for condensation on the inside of the collector's cover plate. This was a rather difficult task, because during the most humid times condensation on the outside of the cover blocked the view. However, no noticeable inside condensation was identified.

The data gives a similar result: no situations were found in which the relative humidity inside the collector would be higher than the ambient relative humidity. Likewise, the dew-point temperature was always lower than the cover temperature. This means that the inside of the collector was drier than the ambient in all cases, and inside condensation did not occur, or was negligible. Hence, the ventilation solution chosen for the Savosolar collector seems to

work well keeping the collector dry.

The outside condensation, as well as dust accumulating on the glass cover, might also pose a problem for the collector efficiency. These issue can probably only be tackled by using a special coating for the cover plate. On sunny days however the condensation vanished during the course of the first 1 - 2 hours after sunrise, so the obstruction caused by outside condensation does not last long.

6 Conclusions

In this thesis, methods for testing flat-plate solar thermal collectors were described. Data for Savosolar's and KBB's solar collectors was gathered by two setups, one for thermal performance and one for microclimate testing. The testing procedure for thermal performance included determining the incoming solar power and the heating power produced by the solar collectors for selected measurement days. The microclimate setup was used to observe the occurrence of condensation on the inside of the collector glazing.

The microclimate setup fulfilled its purpose in pointing out that no considerable inside condensation was found inside the Savosolar collector during the measurement period. The idea of using a diagonal ventilation setup can thus be fully supported. The setup used for conducting thermal performance tests however could not produce sensible results due to the lack of useful data for the heat transfer liquid flow rates. Although the setup does not have to fulfill all the strict requirements for a certified test installation in order to produce results that give an idea about the collector's performance, without the flow rate measurements the heat transfer taking place cannot be evaluated. It is recommended that more sensitive flow meters are used, if the setup's size is to remain the same. If exact results of the collector's thermal performance are needed, consulting a certified testing laboratory is inevitable.

Further research on the thermal performance of the solar thermal collectors requires new flow meters, if the setup is to remain unchanged otherwise. An investigation on how much diffuse irradiance is incident on the collectors could reveal if the white factory wall is responsible for the plateau-shaped irradiance curve measured by the pyranometer. For this purpose another pyranometer, for which the direct beam irradiance is blocked, needs to be introduced into the setup. In order to back up the findings of the condensation setup, another set of measurements with four open ventilation holes (one in each corner) could be performed. If in these measurements inside condensation was found, or if the inside relative humidity was higher than in the measurements conducted for this thesis, it would again stress that the two-hole ventilation is the favourable one.

This thesis has brought new insight into testing methods of solar thermal collectors and will hopefully serve the Savosolar company to develop their product even further. In general, considering the steadily growing competition on the solar collector market, it is recommendable

for start-up companies to include a carefully designed test facility into their planning. With the help of such a test facility, features and characteristics of different collectors can be compared quite accurately, as was attempted to show in this work. A collector that was tested in an official testing laboratory should be taken as the basis of all comparisons. Then the standard sensor equipment for production systems is accurate enough to provide valuable data for research and development purposes. Installing a test bench thus decreases the cost of testing elsewhere and speeds up the development and testing of new products. Although in the very beginning a start-up company does not necessarily have the time and resources to go through such thorough testing as described in this thesis, a well-designed test bench can be a benefit for many years to come.

References

[1] M. King Hubbert, "Nuclear energy and the fossil fuels", Shell Development Company, Exploration and production research division, Publication No. 95, Jun. 1956.

[2] V. Quaschning, "Understanding renewable energy systems". London: Earthscan, 2007.

[3] Savosolar, www.savosolar.fi, last visited on 5.8.2012.

[4] J. A. Duffie, W. A. Beckman, "Solar engineering of thermal processes". 3rd edition, Hoboken: John Wiley & Sons, 2006.

[5] Solar Keymark, www.estif.org/solarkeymarknew, last visited on 5.8.2012.

[6] "Methods for testing to determine the thermal performance of solar collectors", Standard ASHRAE 93-77, 1978.

[7] "Thermal performance of glazed liquid heating collectors", Standard ISO 9806-1, 1994.

[8] "Thermal solar systems and components. Solar collectors. Part 2: Test methods", European Standard SFS-EN 12975-2:en, 2006.

[9] S. Fischer, W. Heidemann, H. Müller-Steinhagen, B. Perers, P. Bergquist, B. Hellström, "Collector test method under quasi-dynamic conditions according to the European Standard EN 12975-2", Solar Energy, vol. 76, pp. 117-123, Jan. 2004.

[10] M. Köhl, V. Kübler, M. Heck, "Optimisation of the micro-climate in solar collectors", Solar Energy Materials and Solar Cells, vol. 91, pp. 721-726, Dec. 2006.

[11] A. Lorenz, "Simulations of the microclimate inside a solar thermal collector", Research report, Renewable Energy Master's Programme, University of Jyväskylä, Jul. 2011.

[12] M. Köhl, B. Carlsson, G. J. Jorgensen, A. W. Czanderna, Ed., "Performance and durability assessment - Optical materials for solar thermal systems". Oxford: Elsevier, 2004.

[13] F. P. Incropera, D. P. DeWitt, T. L. Bergman, A. S. Lavine, "Fundamentals of heat and mass transfer". 5th edition, Hoboken: John Wiley & Sons, 2002.

[14] "Savosolar flat plate collector SF-100-02, Al-fin/Cu tube Absorber" data sheet, Savosolar Oy, Mikkeli, 2011.

[15] "The K4-series standard collectors" data sheet, subsection "K420MS-AL, meander collector with manifolds", KBB Kollektorbau GmbH, Berlin, 2010.

[16] "Tyfocor(R) L" data sheet, Tyforop Chemie GmbH, Hamburg, 2004.